Extraction Optics for Ion Beam Generation in the ARIEL facility at TRIUMF

by

Fernando Alejandro Maldonado Millán
B. Sc., Universidad Autónoma de Yucatán, 2013

A Thesis Submitted in Partial Fulfillment of the
Requirements for the Degree of

MASTER OF SCIENCE

in the Department of Physics and Astronomy

Extraction Optics for Ion Beam Generation in the ARIEL facility at TRIUMF

by

Fernando Alejandro Maldonado Millán
B. Sc., Universidad Autónoma de Yucatán, 2013

Supervisory Committee

Dr. A. Gottberg, Co-Supervisor
(Department of Physics and Astronomy, TRIUMF)

Dr. D. Karlen, Co-Supervisor
(Department of Physics and Astronomy)

Dr. M. Lefebvre, Departmental Member
(Department of Physics and Astronomy)

Supervisory Committee

Dr. A. Gottberg, Co-Supervisor
(Department of Physics and Astronomy, TRIUMF)

Dr. D. Karlen, Co-Supervisor
(Department of Physics and Astronomy)

Dr. M. Lefebvre, Departmental Member
(Department of Physics and Astronomy)

ABSTRACT

The proposed ion optics extraction geometry from ARIEL has been optimized based on simulations with Comsol. Geometrical parameters such as the acceleration gap and angle of the face of the vacuum chamber were studied in order to improve the beam 4-emittance and beam spot size. For geometries of interest, additional studies have been performed: voltage dependence, mass dependence, and the effect of the ion source misalignment on the beam parameters and how to compensate them. Simulations and experimental measurements were also performed for the current ISAC surface ion source to corroborate the simulation results.

Contents

List of Tables

List of Figures

ACKNOWLEDGEMENTS

I would like to thank:

Anders Mjøs and Aaron Schimdt, for helping in performing the experiments.

Alexander Gottberg, for support, encouragement, and patience.

Dean Karlen, for support and advises throughout my degree program.

University Of Victoria, for funding me with a Scholarship.

TRIUMF, for letting me being part of the ARIEL project.

DEDICATION

To my wife, for her love and support during all this adventure. To my family, whom despite the distance, were always close to me.

Chapter 1

Introduction

TRIUMF is a particle and nuclear physics laboratory located in Vancouver, Canada and is one of the leading laboratories for studying rare isotopes.

At the heart of the TRIUMF facility is the largest cyclotron in the world, capable of delivering a proton beam with an energy up to 500 MeV to produce, besides others, Rare Isotope Beams (RIBs).

In an Isotope Separation On Line (ISOL) facility, RIBs are produced by nuclear reactions in a thick target such as uranium carbide. The reaction products diffuse out of the target into the ion source. The ions produced, are extracted by means of an ion optics system, such as an electrostatic lens, and finally are analyzed by a mass separator magnet which selects the desired species [10]. The RIBs at TRIUMF are produced by fragmentation, spallation, and fission reactions inside the target material with a direct impact of the proton beam [17].

As highlighted in TRIUMF's five-year plan 2015-2021 [14], TRIUMF will expand its capabilities of producing RIBs with the Advanced Rare IsotopE Laboratory (ARIEL). Currently, TRIUMF has only one proton driver for two target stations for RIBs in the Isotope Separator and Accelerator (ISAC) facility. ARIEL will add two new target stations and a new driver beam.

The ARIEL Proton Target West station (APTW) will use proton-induced nuclear reactions in ISOL targets by adding a new proton beamline from the main cyclotron. The ARIEL Electron Target East station (AETE) will use an electron-driven photofission ISOL target using the new electron linear accelerator. Both stations will produce short-lived rare isotopes that will be sent to the existing ISAC facility. This will provide the capability for simultaneous delivery of up to three RIBs.

The production of RIBs with the new electron driver beam relies on the process known as photofission. In this process a high energy electron beam is stopped in a converter which creates high energy bremsstrahlung photons that induce fission in the target material.

The first stage of the ARIEL project has completed the construction and commissioning of the electron linear accelerator as well as the building that will house the two new target stations. The electron linear accelerator currently operates up to an energy of 25 MeV and is designed to eventually reach 50 MeV. The acceleration is achieved through superconducting accelerator cavities, operating at 1.3 GHz and at a temperature of 2 K.

The scope of this thesis is to characterize and optimize the design of the new ion extraction optics for ARIEL, and to characterize ISAC's current geometry of extraction and measure its beam parameters experimentally.

In chapter two, the design requirements of ARIEL are stated and a general description of ion sources and ion extraction optics is given. The formulas presented here define the property known as emittance, an important parameter indicating the quality of the beam. In chapter three, general aspects of ion transport simulations are explained. Chapters four and six give the simulation results for the ISAC and ARIEL ion optics respectively. In chapter five, the experimental results to benchmark the simulations for ISAC are described. Finally, conclusions are presented in chapter seven.

Chapter 2

ARIEL and Ion Extraction Concepts

The first stage, ARIEL-I, consisted of the civil construction of the facility and the construction and commissioning of the electron linear accelerator with a beam energy up to 25 MeV.

The second stage, ARIEL II, includes:

- Installation of two target stations: AETE for electron bombardment and APTW for proton bombardment.
- Installation of the remote handling systems necessary for operating the two target stations.
- Installation of a beamline from the cyclotron to APTW.
- Installation of a beamline from the e-linac to AETE.
- Installation of low energy ion beam transport that includes the mass separation device, charge breeding capability and beamlines to deliver ions from ARIEL to the RIB beamlines in ISAC.

Once the isotopes are created inside the target material, they undergo diffusion and effusion in the target bulk material until they reach the ion source transfer tube. It is at this point when the species get ionized. As there is no single ion source capable of ionizing all species, several types of sources are used. A brief explanation of the ion sources used at ISAC is below [4].

The Surface Ion Source (SIS) (fig. 2.1) requires that the energy of ionization of the species of interest is low, which allows the absoprtion of the outermost electron of the species by the metal surface of the ion transfer tube [9]. Typical materials used for the ion transfer tube are tantalum, tungsten or rhenium. The metal operates at high temperature, around 2000° C. This type of source is highly efficient for elements of ionization energy of around 6 eV or below. Many of the ions of interest for ARIEL, such as ^{8}Li, can be obtained with this type of ion source. As a result, the extraction concept studied throughout this thesis corresponds to the ion extraction of a SIS.

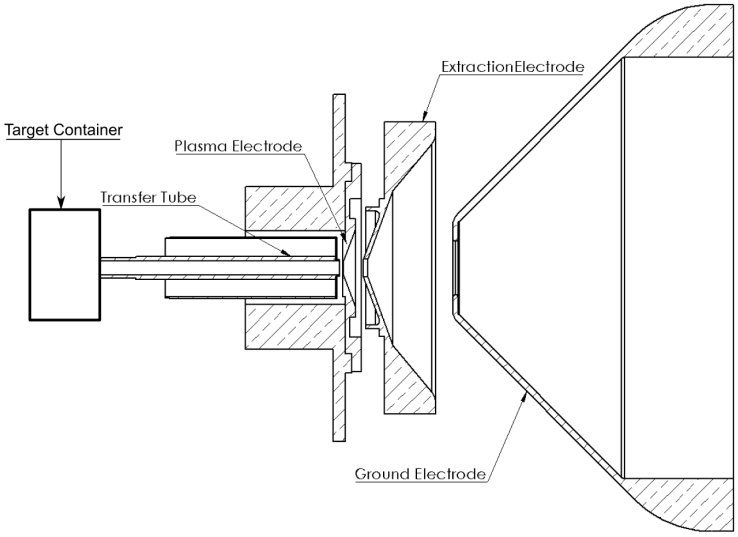

Figure 2.1: Surface ion source used at ISAC with three electrodes for extraction.

The Resonant Ionization Laser Ion Source (RILIS) is in principle similar to the SIS but with the addition of a set of laser beams introduced into the transfer tube. The laser wavelengths are chosen to match excitation and ionization energies of the species of interest.

Another ion source to be used is the IGLIS, the Ion Guide Laser Ion Source. This is almost the same as the RILIS, in the sense that lasers are used to ionize the species. The difference lies in the suppression of unwanted species coming from the surface ionization. To accomplish this, the undesired ions from the SIS are stopped by a repeller electrode and after this, purely laser ionized species are produced and guided by a radio-frequency (RF) quadrupole field.

The last type of ion source foreseen for ARIEL is the Forced Electron Beam Induced Arc Discharge (FEBIAD) (fig. 2.2). This source is capable of ionizing all

elements independent of their ionization energy and consists of a tube that transfers isotopes into a chamber filled with electrons that were previously accelerated to a kinetic energy of around 200 eV and confined with a magnetic field. The isotopes are ionized by collision with the electrons and are extracted through an aperture of the plasma chamber.

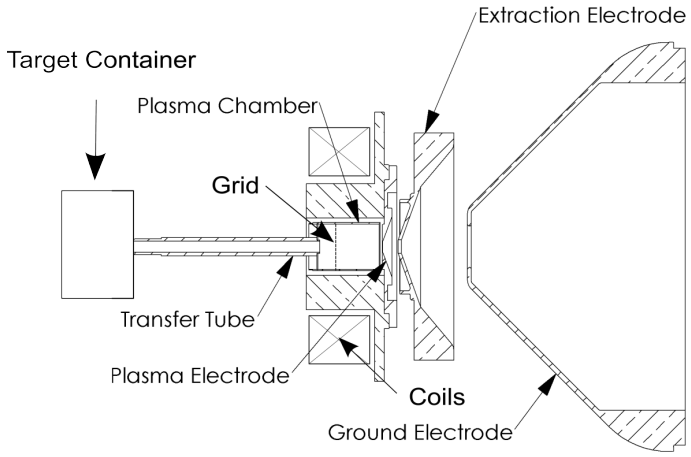

Figure 2.2: FEBIAD source used at ISAC. The coils generate a magnetic field that confines the electrons inside the plasma chamber.

Table 2.1 shows some isotopes of interest for the second stage of ARIEL and the type of ion source used for each species.

Table 2.1: RIBs for ARIEL.

Isotope	Source type
^{8}Li	SIS
^{100}Rb	SIS
^{98}Sr	SIS/IGLIS
^{98}Kr	FEBIAD
^{144}Ba	SIS/IGLIS
^{146}Xe	FEBIAD
^{150}Cs	SIS

Once the ions are generated, independent of the type of source used, the next step is to extract them. This is accomplished by applying a high voltage between the ion source and an extraction electrode. ISAC uses three electrodes fixed in space

and ARIEL plans to use a moveable electrode to match the space requirements of distinct ion sources in the limited area of the vacuum chamber (A. Gottberg, personal communication, 2016). The trajectories of the extracted particles are influenced by the electric field strength and the shape of the electrodes. The particle trajectories determine the beam quality [5] and can be assessed by means of the emittance. The emittance, defined as the six-dimensional volume of the beam in phase space ($x-p_x$, $y-p_y$, $z-p_z$), is conserved when linear and conservative forces are applied [18]. When the longitudinal momentum (p_z) is larger than the transverse momentum, a typical case in accelerators, the area of each transverse phase space is conserved. Moreover, if the system presents cylindrical symmetry, the emittance of each transverse direction is identical and this single value is sufficient to characterize the quality of the beam. The longitudinal emittance is of importance for pulsed beams, such as electron guns and not the case for ion sources, and hence is not take into consideration in the thesis. Furthermore, with the particles traveling in the z direction, each of the areas in the so-called trace space plane $x - x'$ and $y - y'$ are conserved. Here x is the horizontal transverse direction and $x' = p_x/p_z$, where p_x and p_z are the horizontal transverse and longitudinal momentum respectively. The dimensionless parameters x' and y' are typically quoted in milliradians (mrad). The position is commonly quoted in millimeters giving the emittance units of millimeter-milliradian, or mm-mrad for short notation. It can also be quoted as μm given the fact that the radian is unitless. This will be the choice used in the thesis when quoting emittances.

An important remark is that the area of the phase space is conserved, regardless of its shape (fig. 2.3), however, an elliptical shape is always desired as is it less prone to suffer losses during transportation [5]. Furthermore, a smaller value indicates a better beam; however, other aspects to take into account in the design are the transmission of the ion beam through the beamline elements, as well as its beam size.

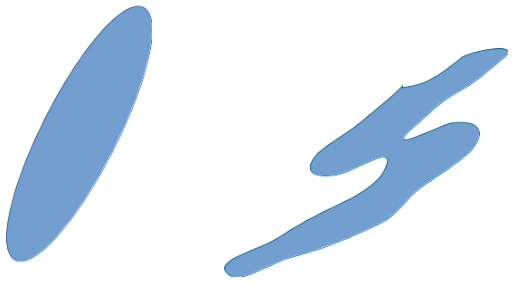

(a) Elliptical. (b) *S-shaped.*

Figure 2.3: Typical transverse phase space diagrams with the same area.

When reporting values of emittance, the common practice is to report the 4 - emittance (4ϵ). This guarantees that a large fraction of the beam is contained within the area.

The 4-emittance of a SIS with a circular aperture can be estimated using equation 2.1 [13]. This equation assumes the ions follow a Maxwellian velocity distribution.

$$4\epsilon = \frac{0.0653}{\beta\gamma} \cdot r \cdot \sqrt{\frac{kT}{M/Q}} \quad [\mu\text{m}] \tag{2.1}$$

Here r is the radius of the ion source aperture, in mm. kT is the energy in eV of the ion due to the temperature of the ion source transfer tube with k being the Boltzmann constant, and M/Q is the mass to charge ratio in units of amu.

$\beta\gamma$ are the relativistic parameters. They depend on the voltage and can be calculated as follows

$$\gamma = (1 - \beta^2)^{-1/2}$$

and

$$\beta = 1.46 \times 10^{-3}(V/M)^{1/2}$$

Where V is the high voltage used for the extraction, in kV. From the the ARIEL design requirements [12][3] the nominal high voltage is 60 kV and the aperture radius of the surface ion source is r=1.5 mm. This leads to a theoretical 4-emittance of around $4\epsilon = 4$ μm.

The basic idea of the extraction system for ARIEL is to have the ion source and a part of the vacuum chamber at high voltage and the rest at ground, with an insulator between them. The ground electrode is located inside this chamber (fig. 2.4).

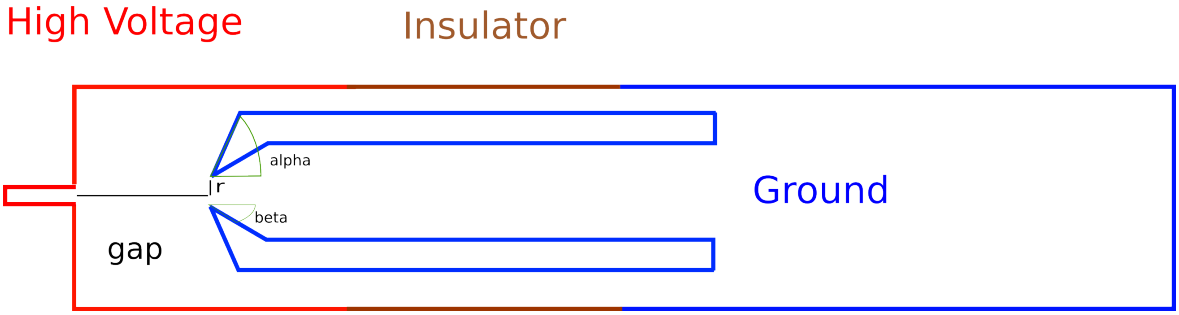

Figure 2.4: Schematic design of the extraction optics and key geometric parameters.

The distance between the exit of the ion transfer tube and the hole of the extraction electrode is called the "acceleration gap" (fig. 2.4).

Chapter 3

Ion Optics Simulations

The radioactive ion beam properties are modeled using a particle tracking simulation. In order to obtain the position and velocity of the ions, the geometry of the conductors and their electric potentials are setup to define the electric fields which accelerate the ions.

The geometry of interest is drawn in Solidworks [2]. The components of the system are the chamber and either a single extraction electrode (ARIEL) or multi-stage extraction electrodes (ISAC). The chamber provides a vacuum environment for the ions to pass through.

Comsol Multiphysics [1] is a finite element analysis software, used to simulate several physics processes (fig. 3.1). Comsol has many *physics* modules, such as heat transfer and fluid flow. For the purpose of this thesis, only two modules are used from the AC/DC category: Electrostatics and Charged Particle Tracing. The first module models static electric fields, such as those used in the ARIEL and ISAC extraction optics. The second module computes the trajectory of charged particles inside an electromagnetic field computed by the first module. LiveLink is another module that is used to connect Comsol and Solidworks. With LiveLink, an open model in Solidworks can be used as a geometry definition in the Comsol interface. This feature allows to have a dynamic geometry, that is, to be able to change the geometry in Solidworks as part of the Comsol study. LiveLink also allows variables defined in Solidworks to be passed to Comsol.

Once this link has been set and all the physics is established, a parametric sweep is performed, that is, a repetitive calculation while changing the value of a certain variable. For instance, a sweep on the variable corresponding to the acceleration gap, will fix it to an initial value, then calculate the corresponding electric field, release

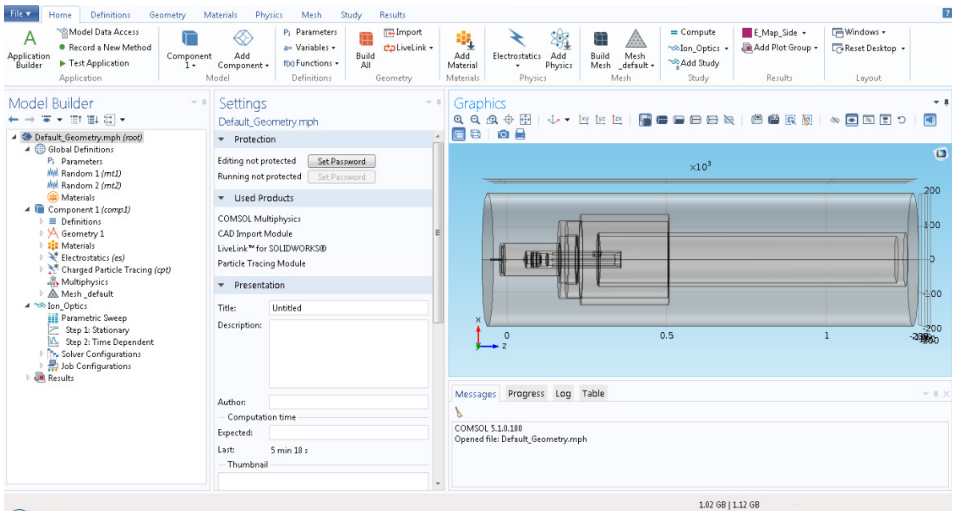

Figure 3.1: Comsol main interface showing the imported geometry.

particles and track them, export the results, and then repeat with the next value for the acceleration gap.

3.1 Methodology of the simulations

In the electrostatics setup of the Comsol interface, metal surfaces are set to specific potentials as boundary conditions and the electric field is calculated within the vacuum chamber.

In the charged particle tracing configuration, the field computed in the electrostatic study is used as input. The masses and charges of the ions are fixed and their positions and velocities are updated in time steps of 1 ns, allowing the emittance of the beam to be calculated at various locations. The total time for tracking was set to 30 μs.

The size of the mesh was selected from a pre-defined configuration suggested by Comsol based on the modules selected. The size of this pre-defined configuration, however, was reduced until the results did not varied due to the size of the mesh. Preliminary simulations were computed with 3000 particles for the default ISAC geometry using [16] as reference for the beam properties obtained.

3.1.1 Particle generation

Different choices for distributing the initial particle positions and velocities lead to different results when compared to [16]. Three possibilities were considered: uniform distribution on the surface of a disc, uniform distribution from the inner surface of the ion transfer tube, and uniform distribution within the inner volume of the ion transfer tube.

Disc generation

This configuration has the particles distributed uniformly from a metal disc located at the downstream end of the ion transfer tube (fig. 3.2). The disc is held at the same potential of the chamber and the initial kinetic energies of the particles follow a Maxwellian distribution at 2000°C. The direction of each particle is assigned randomly over a half sphere. This configuration is an oversimplifaction as it doesn't take into account the beam formation due the electric field that exists inside the ion transfer tube (fig. 3.3) and it also dramatically changes the field downstream of the ion tube. Hence, it is not surprising that this configuration leads to discrepancies with the reported values in [16].

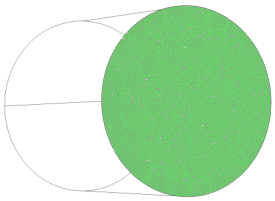

Figure 3.2: Disc for particle generation.

Inner surface

Figure 3.4 depicts the surface for particle generation and figure 3.5 shows the initial distribution for this configuration. The direction vector of each particle is randomly chosen from a uniform distribution over a half sphere defined by the vectors of fig. 3.4. The particles are assigned a fixed kinetic energy equal to 0.292 eV (thermal energy at 2000°C).

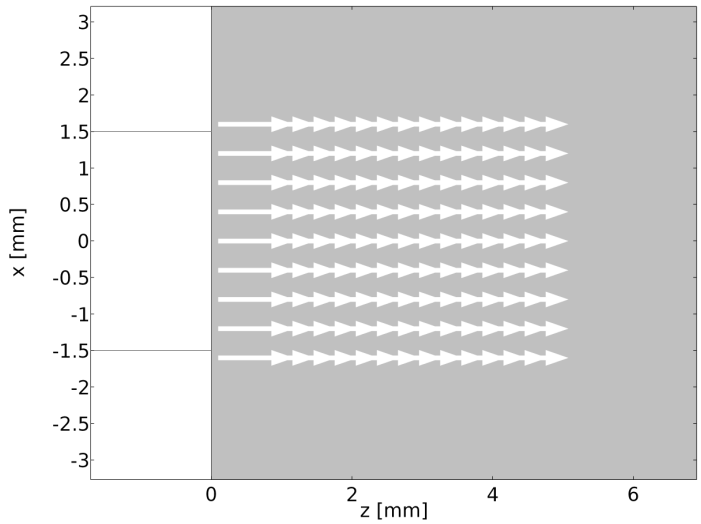

(a) Electric field grid from a disc.

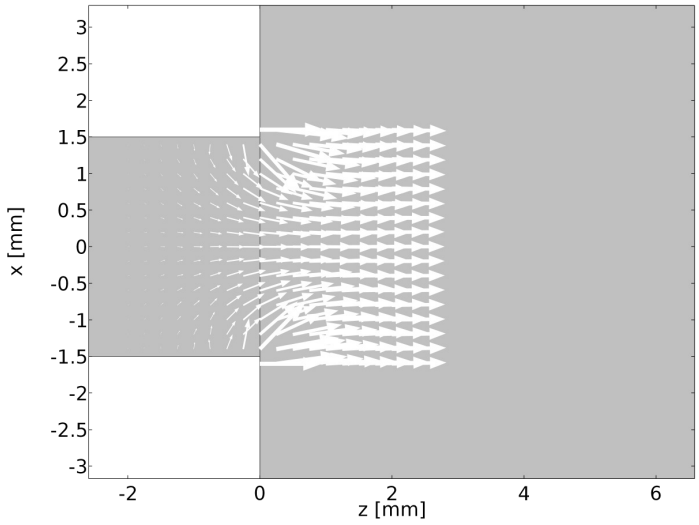

(b) Electric field grid from a tube.

Figure 3.3: Electric field computed for two different boundary conditions. The electric field is computed only in the gray area. Field strength is indicated by both vector length and line thickness.

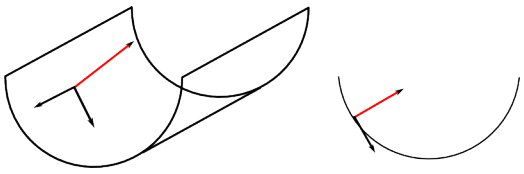

Figure 3.4: Particle direction generation in the surface of a cylinder.

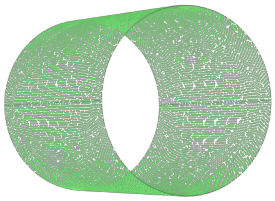

Figure 3.5: Surface for particle generation.

The program requires that surfaces be modelled with a mesh, which is not a good representation of a cylinder. This results in electric fields at the surface that imparted unphysical energies to the particles.

Inner Volume

This configuration uniformly populates the vacuum inside the ion transfer tube with particles (fig. 3.6). The initial kinetic energy follows a Maxwellian distribution at 2000°C and the initial directions are uniform in half a sphere.

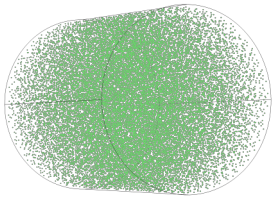

Figure 3.6: Volume for particle generation.

When the simulation was performed with this initial distribution for particles, results agreed with the reported values in [16].

With this agreement, a new study with the ISAC geometry was performed by varying the high voltage and the number of electrodes (fig. 2.1) . These configurations were measured experimentally (chapter 5) to fully corroborate the simulations explained in chapter 4.

3.2 Data analysis

Due to the large amount of data generated by the simulations and limitations of Comsol, scripts were written in ROOT [6] to analyze the data. They can read different files and distinguish between specific sets of data inside those files, allowing an easier way to manipulate the data, particularly when calculating the emittance. Plots of the simulation results are generated by ROOT during the analysis.

The 4-emittance of the beam in the x direction is calculated using

$$4\epsilon^{x}_{rms} = 4\sqrt{V_x V_{x'} - V^2_{x\cdot x'}} \quad [8] \tag{3.1}$$

where V_x is the variance of the horizontal transverse direction distribution x, $V_{x'}$ is the variance of the angle distribution x' with $x' = p_x/p_z$, being p_x and p_z the transverse and longitudinal momentum respectively, and $V_{x\cdot x'}$ is the covariance among both distributions. The same relation holds for $4\epsilon^{y}_{rms}$, with the vertical direction y and $y' = p_y/p_z$, and is identical to $4\epsilon^{x}_{rms}$ due to the cylindrical symmetry of the systems studied.

The transmission efficiency is defined as the fraction of ions exiting the ion source tube that arrive at the downstream wall of the chamber. Finally, the beam size is defined as the full width at half maximum of the one dimensional position distribution, at the same downstream end position.

Chapter 4

ISAC Ion Optics Simulation Studies

Simulations were performed for the ISAC surface ion source for rubidium ions (85 amu). Beam properties are computed for different extraction voltages and for different geometries, such as one without the plasma electrode. In chapter 5, these simulations results are compared to experimental measurements.

4.1 Default geometry

The default ISAC's extraction optics geometry consists of three electrodes: the plasma electrode, the extraction electrode and the ground electrode (fig. 2.1).

The plasma electrode and the ion transfer tube are set to 30 kV and the extraction electrode is set to a lower voltage and the difference is called extraction voltage. The nominal value for the extraction voltage is 1.5 kV, for which the extraction electrode potential is 28.5 kV. The extraction voltage is swept through the values shown in table 4.1.

Table 4.1: Range of values considered for the extraction electrode voltage.

Parameter	Values	Comment
Extraction voltage	0-3 kV	steps of .25 kV

The electric potential in the vacuum is computed with the applied boundary conditions of the electrode voltages. Once the field is computed, particles are distributed

in the vacuum inside the transfer tube as described in section 3.1.1. Figures 4.1, 4.2 and 4.3 show the electric potential and particle trajectories for a few values of extraction voltage. When the extraction voltage is increased, the equipotential surfaces downstream of the ion transfer tube get closer to each other, corresponding to a higher electric field.

Figure 4.1a shows the electric potential of the surface ion source for a configuration without an extraction voltage. The electric potential is practically constant to the left of the extraction electrode. The potential between the transfer tube and the ground electrode creates a weak electric field and when the particles exit the source they are weakly focused. The focal point of the beam (fig. 4.1b)is located approximately at the extraction electrode, mainly because their transverse velocity is comparable to the longitudinal velocity imparted by the electric field. However, the electric potential around the aperture of the extraction electrode ends up over-focusing the beam, and some losses occur in the plasma electrode.

When an extraction voltage is applied, as demonstrated in figure 4.2a, the potential from the plasma electrode to the extraction electrode generates an electric field that focuses the beam near the plasma electrode aperture (fig. 4.2b). When the ion beam reaches the extraction electrode, the electric field in this zone causes a small convergence. This results in a small beam spot at the downstream end.

For an extraction voltage set to 3 kV, the potential in the zone between the plasma electrode and the extraction electrode creates a larger electric field than in previous cases. The beam once again shows a focal point near the plasma electrode and the beam diverges due the strong acceleration caused by the field, see figure 4.3.

The emittance and the beam spot size are calculated downstream of the the ground electrode at a distance of 90 mm from the exit of the ion transfer tube.

The emittance increases as a function of extraction voltage (fig. 4.4). This is caused by the electric field near the ion transfer tube exit that imparts a divergent trajectory. The transmission efficiency indicates that at low voltages some particles strike one of the electrodes. Starting from 1 kV all the particles generated pass through the optics.

The beam spot size at the end of the optics is minimized when the extraction voltage is set to 1 kV (fig. 4.5). This is caused by the electric potential in the extraction electrode restraining the outward spread of the beam.

Figure 4.6 shows the phase space in the x direction for different extraction voltages. The y direction is identical due to the cylindrical symmetry. The shape changes

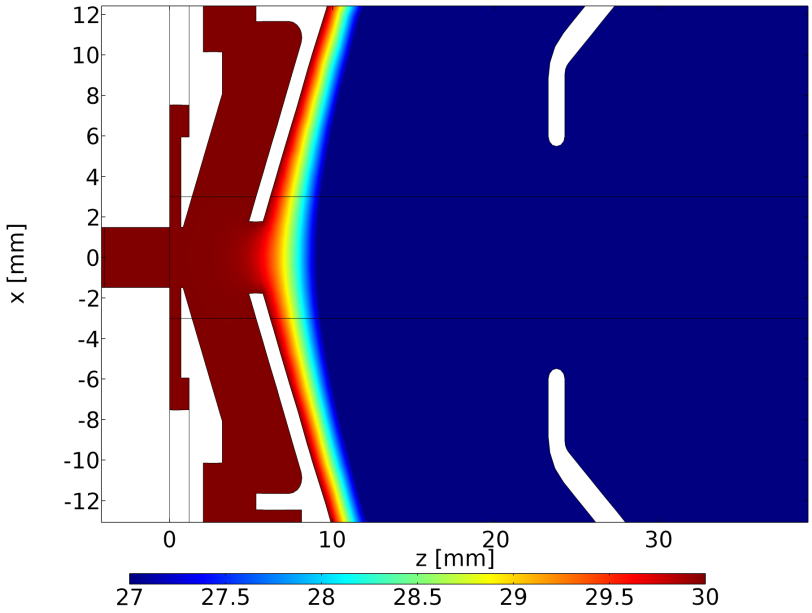

(a) Electric potential and corresponding color scale in kV.

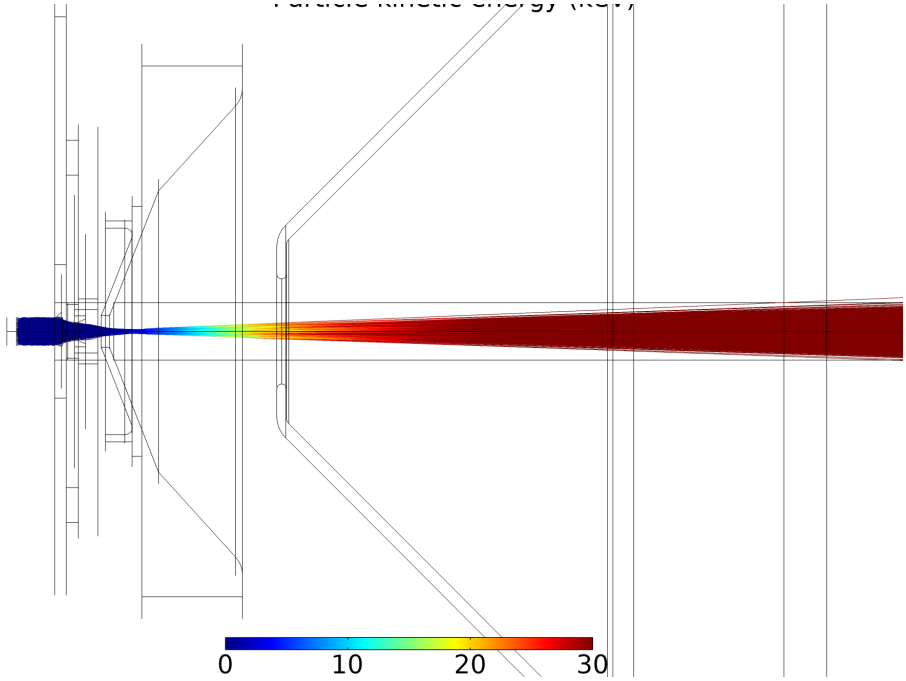

(b) Particle trajectories. The color scale for particle trajectories throughout this chapter indicates particle kinetic energy in keV.

Figure 4.1: Electric potential and particle trajectories with the extraction voltage set to 0 kV for ISAC's default geometry. The color scale of the electric potential within the chamber in the figures throughout this chapter is limited to the range of 27-30 kV in order to better see the changes when the extraction voltage varies.

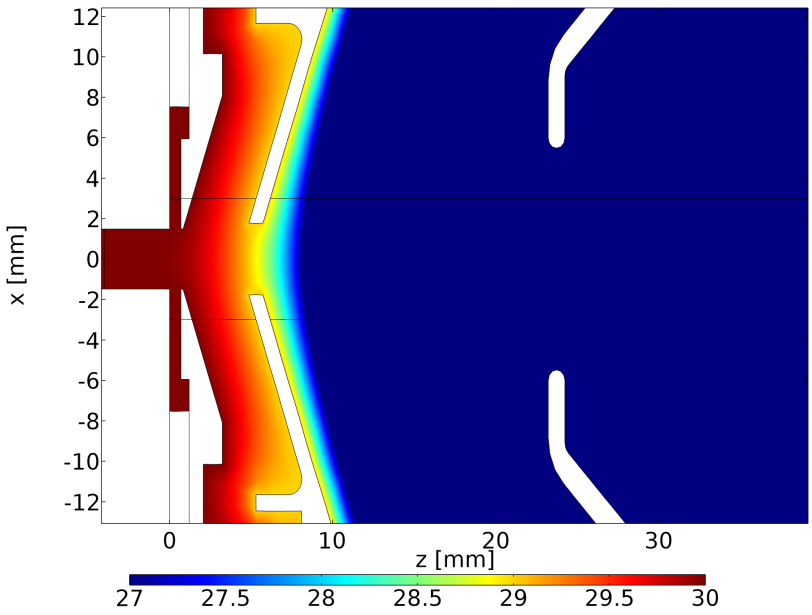

(a) Electric potential

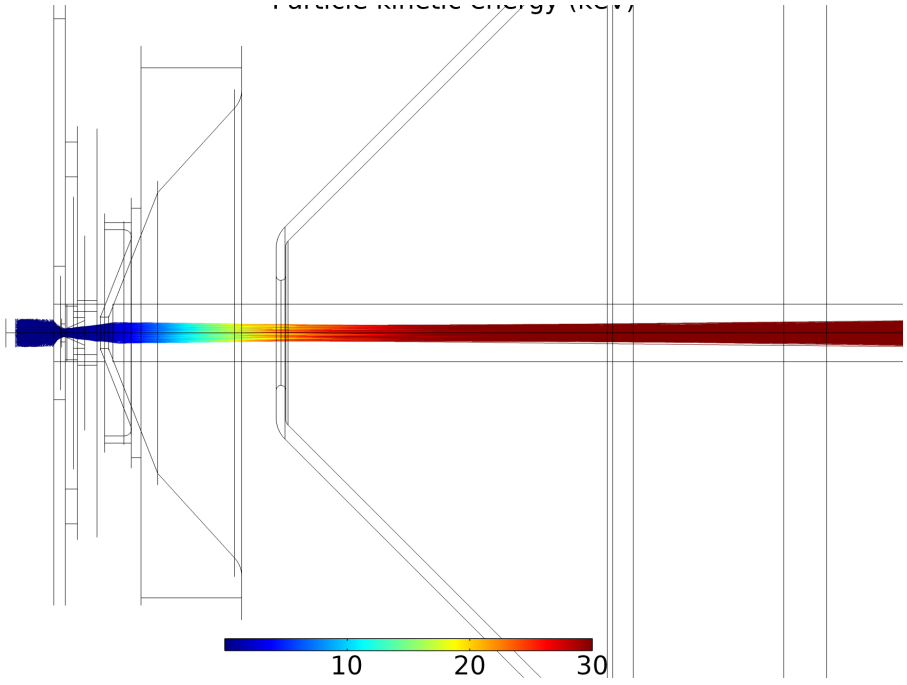

(b) Particle trajectories

Figure 4.2: Electric potential and particle trajectories with the extraction voltage set to 1 kV for ISAC's default geometry.

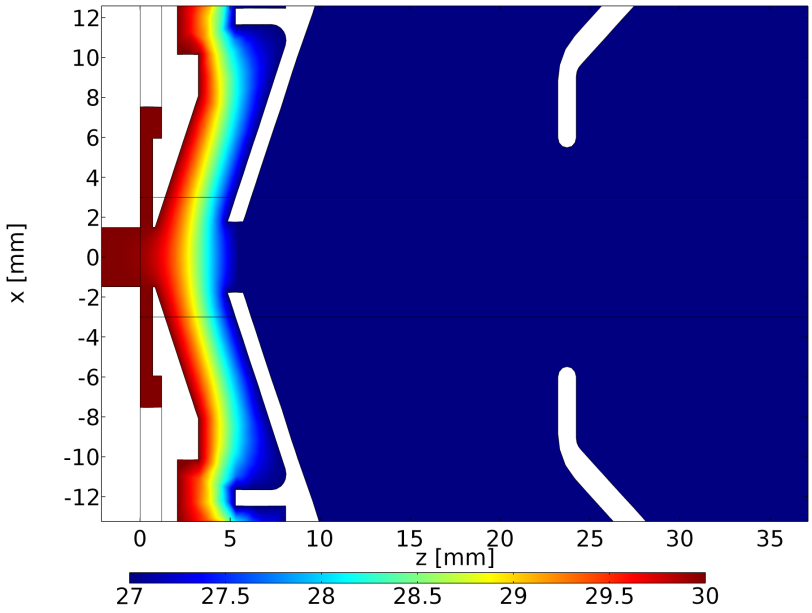

(a) Electric potential

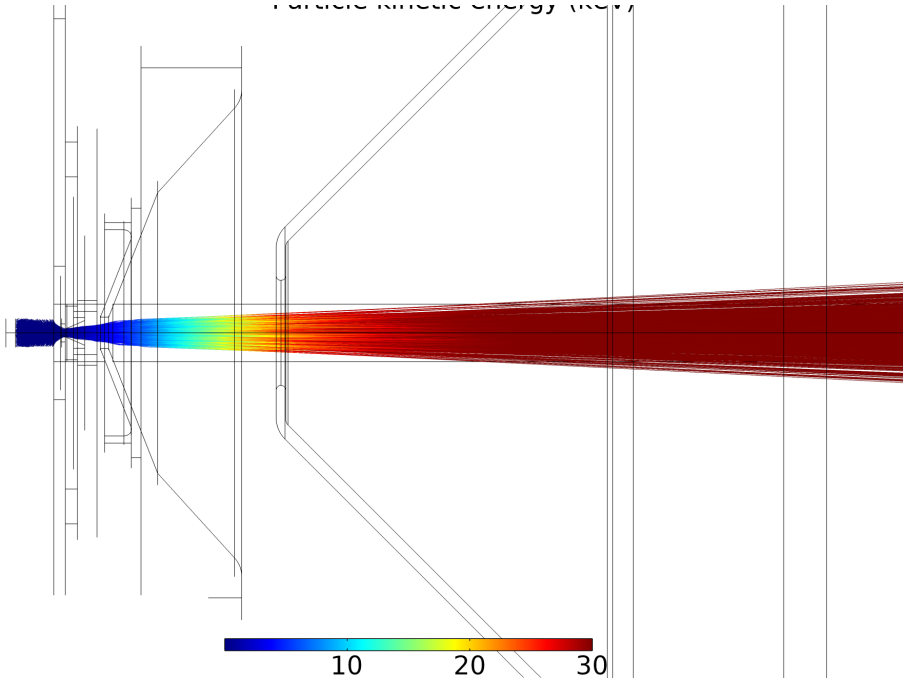

(b) Particle trajectories

Figure 4.3: Electric potential and particle trajectories with the extraction voltage set to 3 kV for ISAC's default geometry.

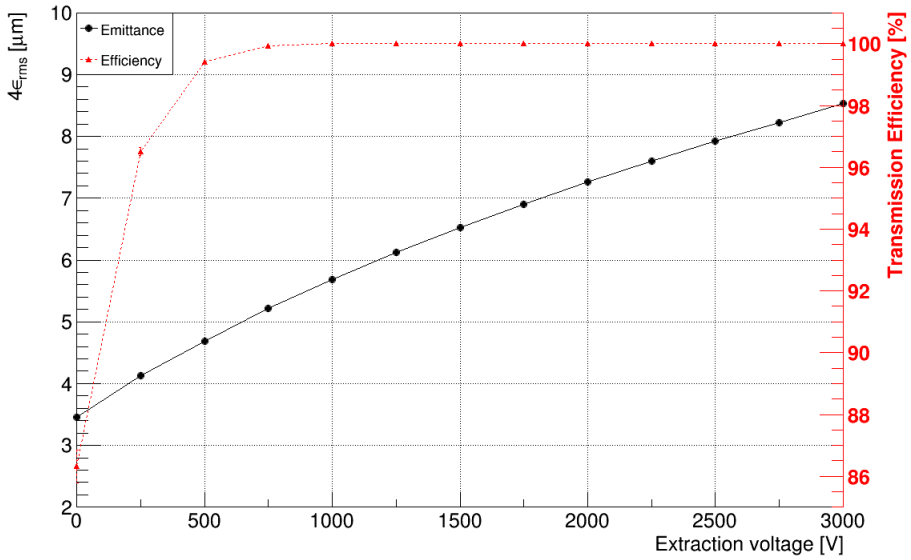

Figure 4.4: Emittance as a funtion of extraction voltage for ISAC's default geometry.

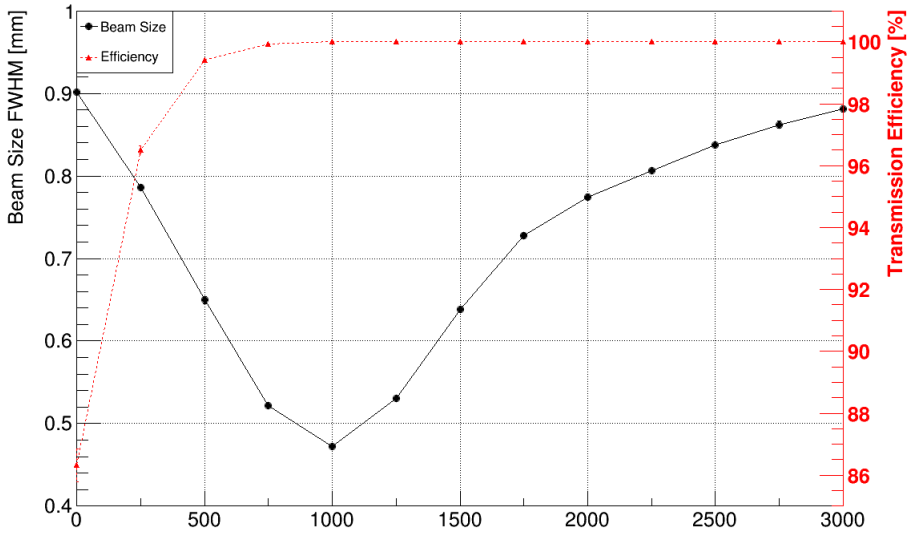

Figure 4.5: Beam spot size as a function of extraction voltage for ISAC's default geometry.

depending of the position distribution and angle distribution and its correlation. The tilt in all images correspond to a beam that is diverging, however, the amount of divergence and beam size is smaller in figure 4.6b and these are desired properties for beam transport.

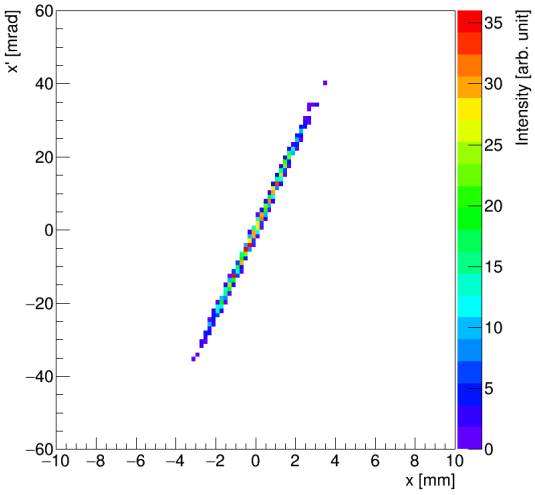

(a) 0 kV, $4\epsilon_{\text{rms}}$=3.45 μm

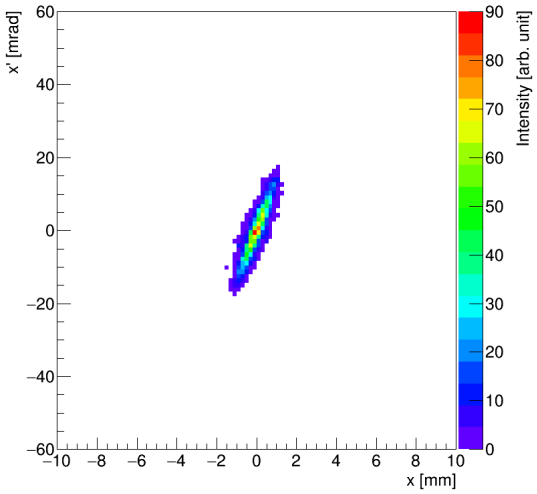

(b) 1 kV, $4\epsilon_{\text{rms}}$=5.68 μm

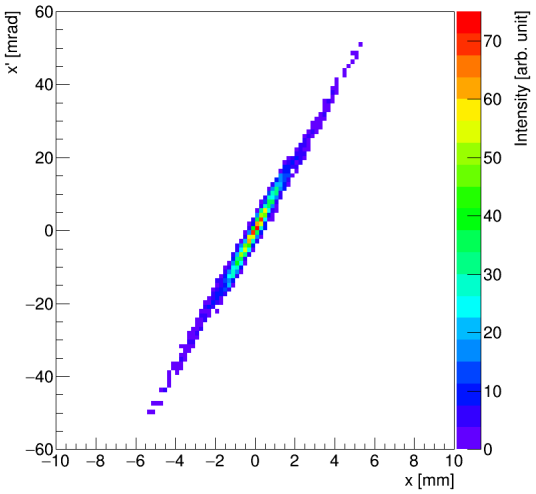

(c) 3 kV, $4\epsilon_{\text{rms}}$=8.52 μm

Figure 4.6: Phase space distribution of particles at the end of the optics, and the corresponding emittances for different extraction voltages with ISAC's default geometry.

4.2 Removed plasma electrode

The same analysis was carried out for a configuration that did not contain a plasma electrode. The color scale of the electrical potential shown is again between 27-30 kV to see more easily how it changes downstream of the ion transfer tube.

When no extraction voltage is applied, the electric potential is approximately constant between the extraction electrode and the ion transfer tube. The beam presents a focal point downstream of the extraction electrode (fig. 4.7).

The equipotential surfaces downstream of the ion transfer tube are approximately planar and perpendicular to the z direction (fig. 4.8a). The corresponding electric field provides only weak focusing.

Figure 4.9 shows the potential downstream of the ion transfer tube for a extraction voltage of 3 kV. The large acceleration induced by the field causes an increase in the spot size.

Just as for the previous geometry, the emittance increases with the extraction voltage, as shown in figure 4.10. The transmission efficiency is 100% for extraction voltages greater than 250 V. For the 0 V case, the ions extracted create a *cloud* at the exit of the ion transfer tube due to their relative small velocity and hence some of this particles do not arrive at the end of the chamber.

The beam size as a function of extraction voltage is shown in figure 4.11. A minimum occurs near 1 kV.

Figure 4.12 shows the phase space for different extraction voltages. The tails in figure 4.12b are the result of some particles diverging more than the overall beam, this type of shape is hard to transport without losses. The particles diverging are most likely to originate near the exit of the transfer tube, and due to the fact that the plasma electrode is absent, their trajectories are affected strongly by the new shape of the electric field.

4.3 ARIEL-like configurations

In these studies the extraction electrode was removed in order to simulate a configuration that can be measured experimentally and which is similar to the proposed ARIEL geometry, but without the foreseen geometry optimization, discussed later. Two cases were computed: with and without plasma electrode.

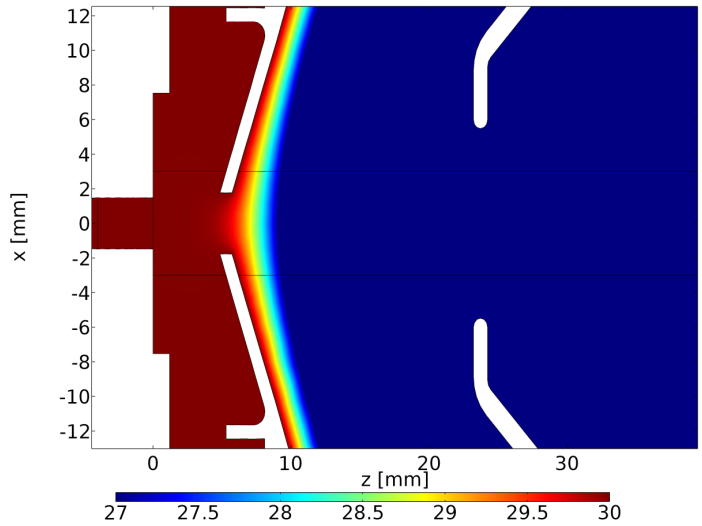

(a) Electric potential.

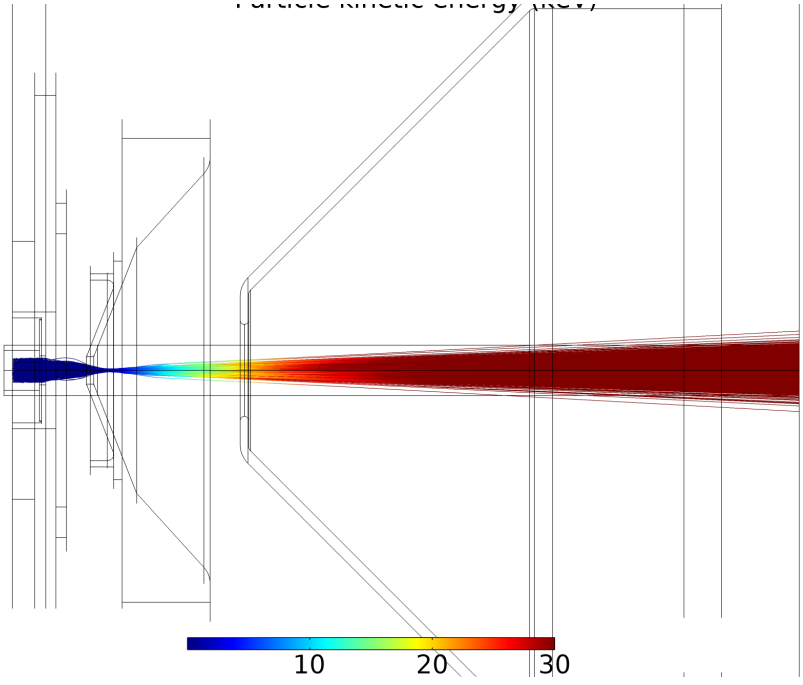

(b) Particle trajectories

Figure 4.7: Electric potential and particle trajectories with the extraction voltage set to 0 kV for ISAC's geometry with the plasma electrode removed.

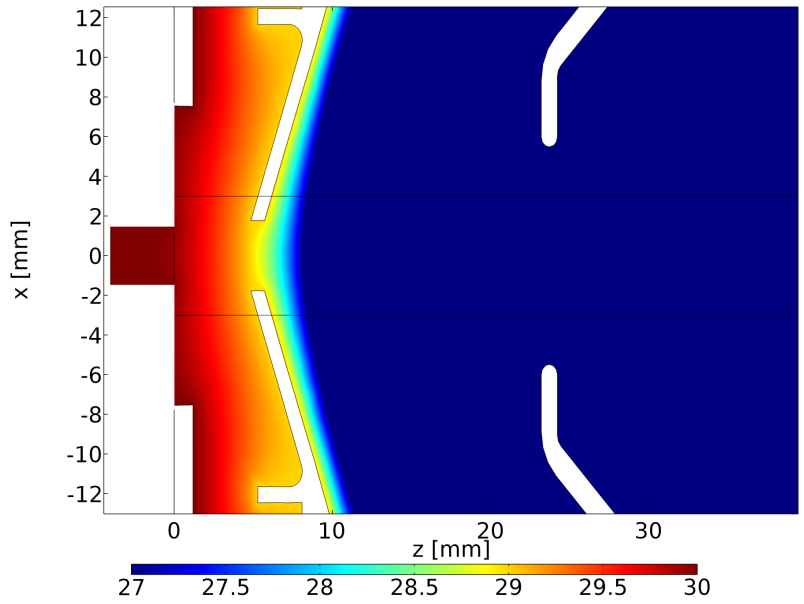

(a) Electric potential.

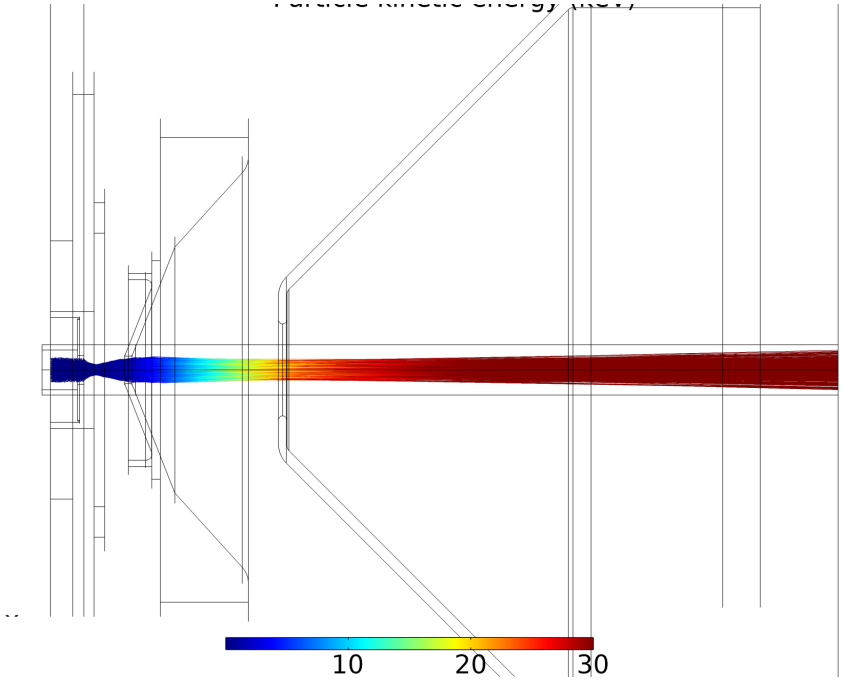

(b) Particle trajectories.

Figure 4.8: Electric potential and particle trajectories with the extraction voltage set to 1 kV for ISAC's geometry with the plasma electrode removed.

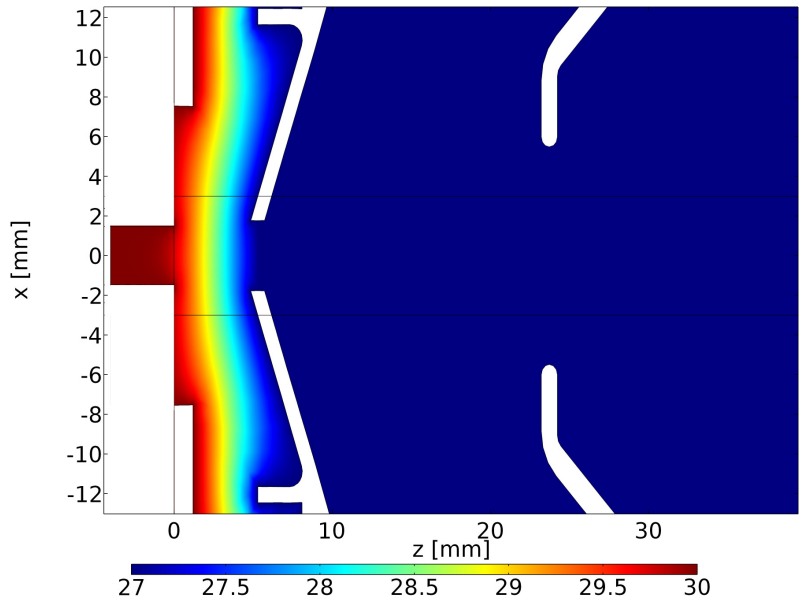

(a) Electric Potential

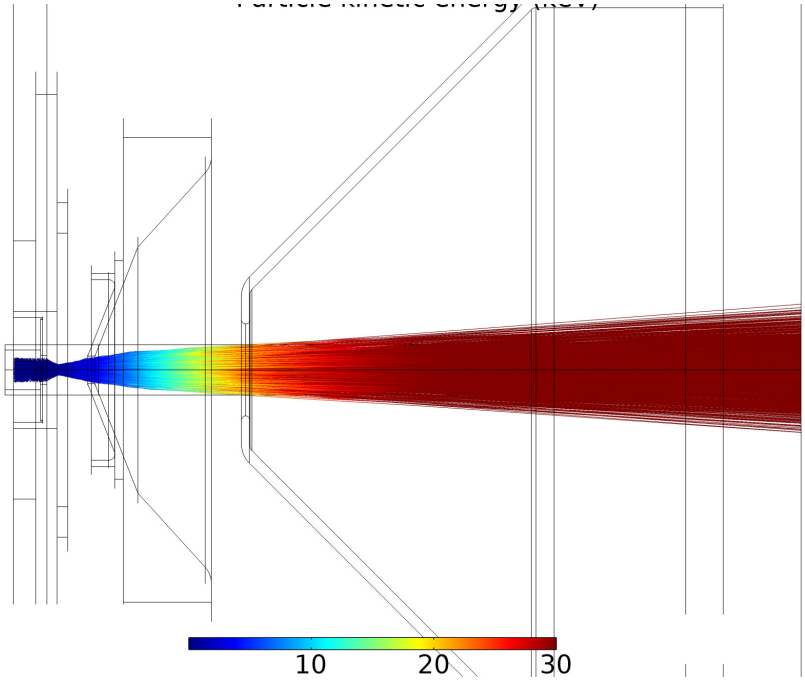

(b) Particle trajectories

Figure 4.9: Electric potential and particle trajectories with the extraction voltage set to 3 kV for ISAC's geometry with the plasma electrode removed.

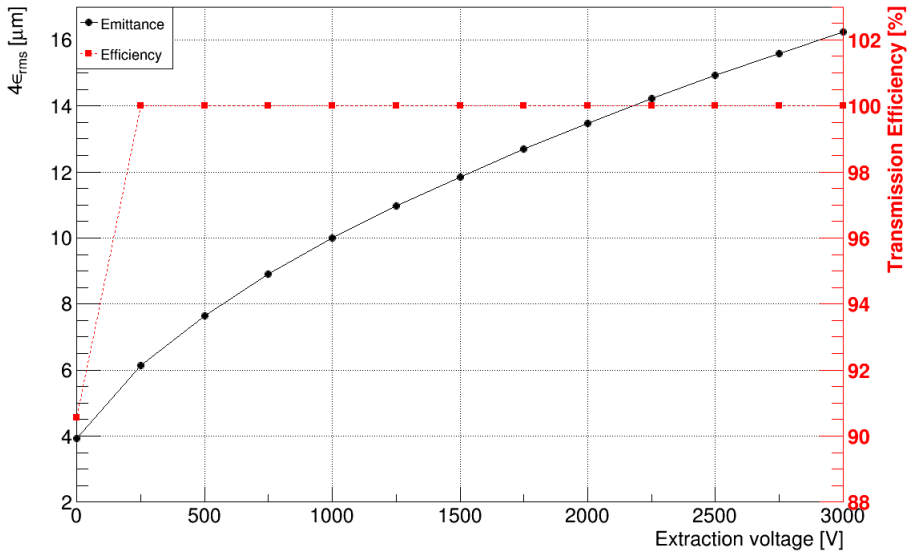

Figure 4.10: Emittance as a funtion of extraction voltage for ISAC's geometry with the plasma electrode removed.

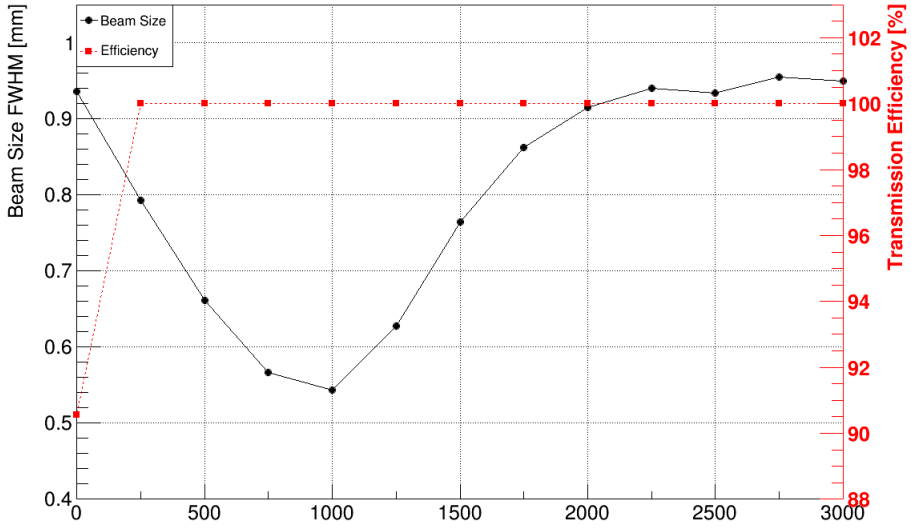

Figure 4.11: Beam spot size as a function of extraction voltage for ISAC's geometry with the plasma electrode removed.

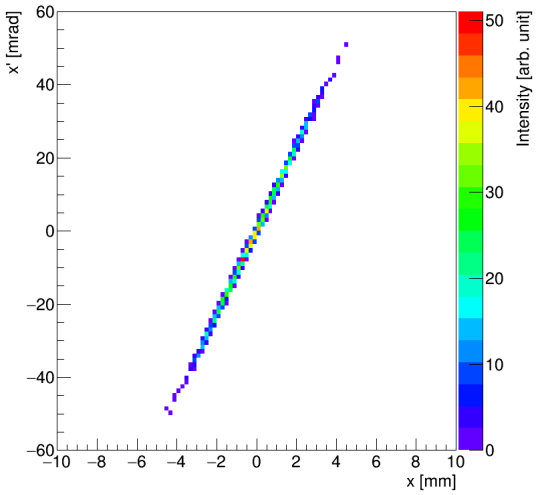

(a) 0 kV, $4\epsilon_{\mathrm{rms}}$=3.80 μm

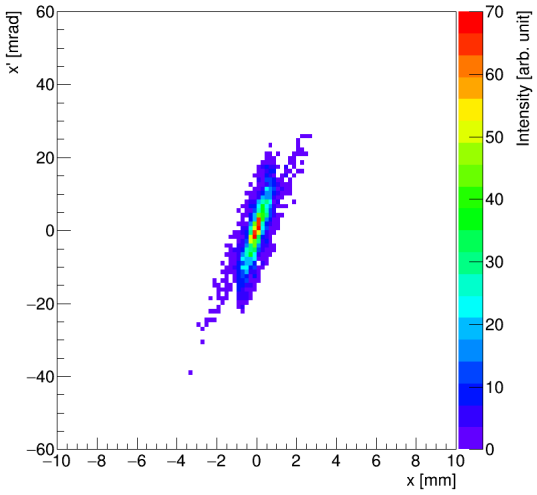

(b) 1 kV, $4\epsilon_{\mathrm{rms}}$=11.76 μm

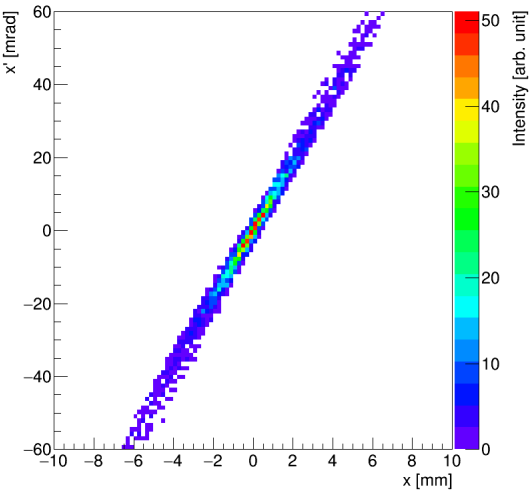

(c) 3 kV, $4\epsilon_{\mathrm{rms}}$=19.13 μm

Figure 4.12: Phase space for different extraction voltages with ISAC's geometry having the plasma electrode removed.

4.3.1 No plasma electrode

The electric potential downstream of the ion transfer tube is similar to ones in section 4.2. In this case, the beam diverges as there is no extraction electrode to impart some convergence (fig. 4.13).

The results of emittance and beam size are presented in table 4.2.

Table 4.2: Beam parameters for ARIEL-like geometry with ground electrode only.

Parameter	Value
$4\epsilon_{\text{rms}}$	21.88 μm
Beam size FWHM	7.45 mm

The phase space (fig. 4.14) shows long tails that contribute to the large value computed.

4.3.2 Ground electrode and plasma electrode

When the plasma electrode is included, the electric field downstream of the ion transfer tube provides some focusing, as shown in figure 4.15b.

The emittance value is shown in table 4.3. The phase space is shown in 4.16 and the tails are shorter for this case.

4.4 Discussion

The emittance almost doubles for large extraction voltages if the plasma electrode is removed as shown in figure 4.17.

The beam size is minimized near 1 kV in both cases and is larger when the plasma electrode was removed (fig. 4.18).

The transmission efficiency, figures 4.4 and 4.10, indicates that the plasma electrode prevents the maximum transmission at low extraction voltages. If the plasma electrode were to be removed from the configuration in order to make use of the high transmission, changing the geometry and/or position of the extraction electrode–or even the ground electrode–could recover low values of the beam parameters now with a higher current.

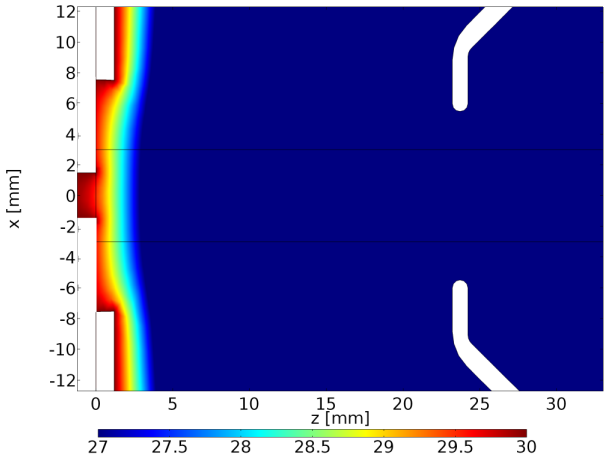

(a) Electric potential

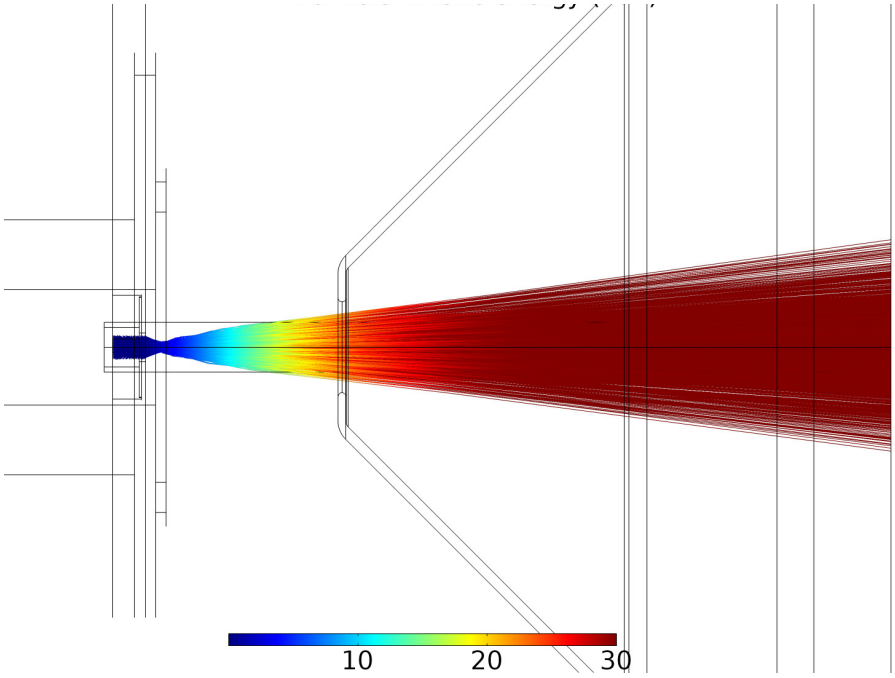

(b) Particle trajectory

Figure 4.13: Electric potential and particle trajectories for ARIEL-like geometry with ground electrode only.

Table 4.3: Beam parameters for ARIEL-like geometry with the plasma electrode added.

Parameter	Value
$4\epsilon_{\text{rms}}$	9.31 μm
Beam size FWHM	3.68 mm

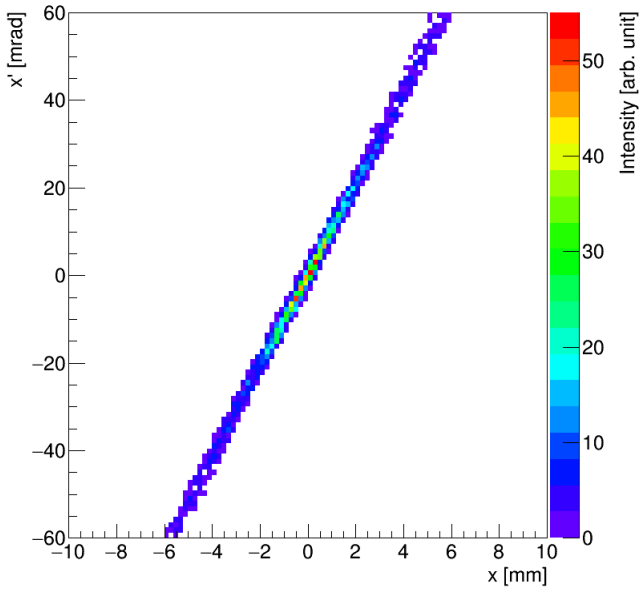

Figure 4.14: Phase space for ARIEL-like geometry with ground electrode only.

Finally, for the ARIEL-like geometries, the emittance is approximately 2.5 times larger and the beam size 50 % larger if the plasma electrode is not present (table 4.4).

Table 4.4: Beam parameters for ARIEL-like configurations.

Parameter	Ground only	Plasma plus ground
$4\epsilon_{\mathrm{rms}}$	21.88 μm	9.31 μm
Beam size FWHM	7.45 mm	3.68 mm

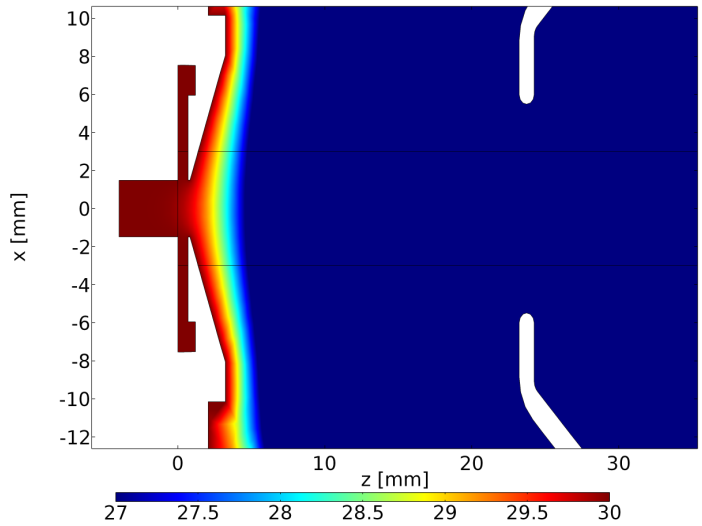

(a) Electric potential.

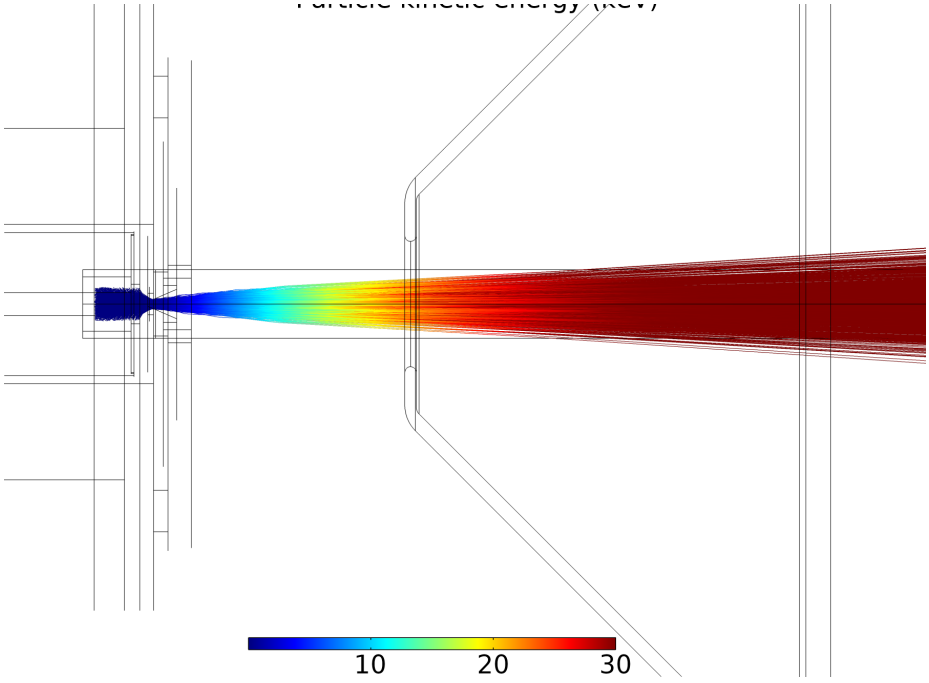

(b) Particle trajectory.

Figure 4.15: Electric potential and particle trajectories for ARIEL-like geometry with the plasma electrode added.

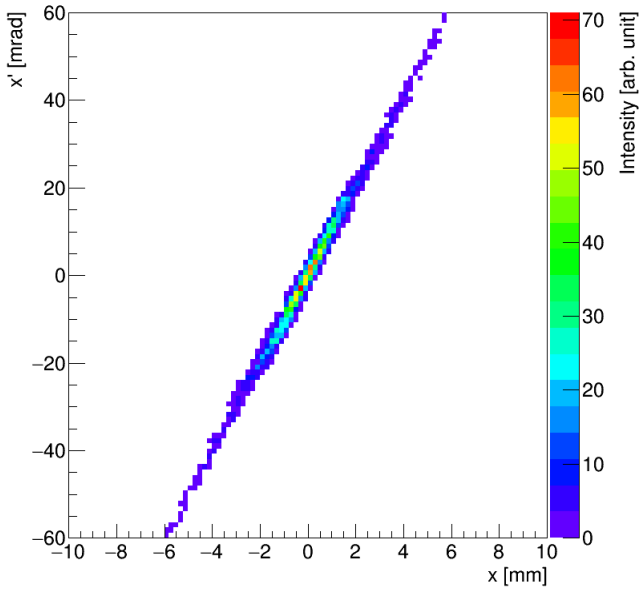

Figure 4.16: Phase space for ARIEL-like geometry with the plasma electrode added.

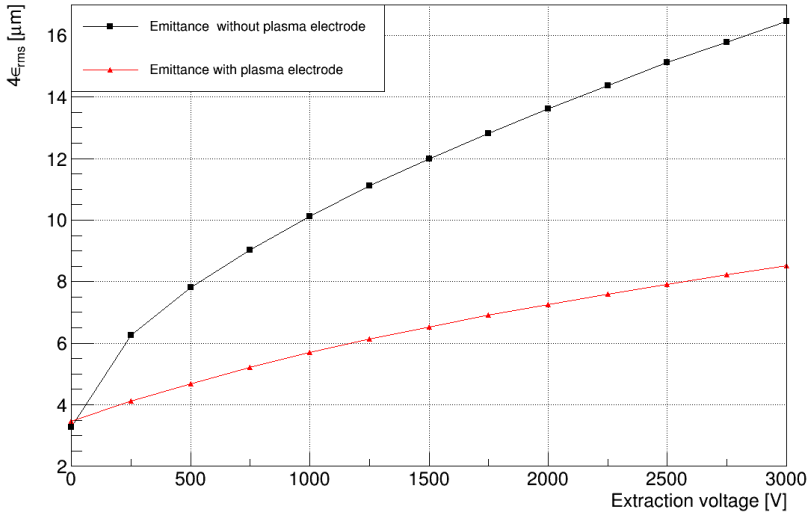

Figure 4.17: Emittance for ISAC's geometry with and without the plasma electrode.

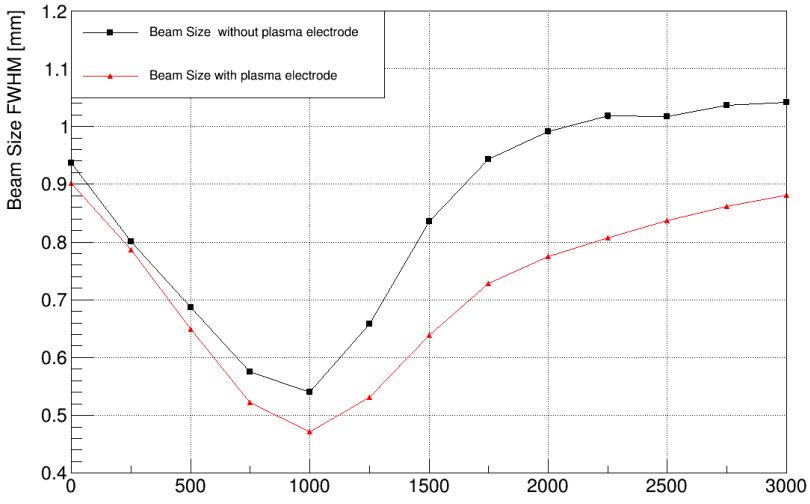

Figure 4.18: Spot size for ISAC's geometry with and without plasma electrode.

Chapter 5

ISAC Test Stand Experiments

To verify the simulations shown in chapter 4, beam properties were measured at the ISAC test stand [7]. The test stand consists of a replica of the relevant parts of the target module in the ISAC facility together with a beam transport line and beam diagnosis devices. The beamline total length is 5 m. The separation of species is achieved using a dipole magnet, as described below. The test stand allows the emittance and beam size to be measured and it can be used to test new geometries for ion beam extraction. It has the capability to run tests on ion sources such as FEBIAD or SIS.

Preliminary tests were done to check the production and transmission rates of a number of ions released from a mixture of salts (table 5.1). The mixture was poured into the ion transfer tube in order to be deposited on the interior surface [15]. When heated, the ions are generated and subsequently extracted.

Table 5.1: Values use in the mixture of salts for preliminary tests.

Element	Volume [μL]	Mass (amu)
Lithium	5	7
Sodium	5	23
Potassium	5	39
Rubidium	5	85
Cesium	5	132

Figure 5.1 shows the injection of a rubidium solution into the ion source container through the back of the extraction electrode with the aid of an autopipette. This procedure is repeated for all the salts with a clean new tip to avoid cross contamination

of the solution bottles. The container is tilted and rotated manually in order to distribute the salts as uniformly as possible over all of the internal surface of the ion transfer tube.

(a) Rubidium salt taken from a solution.

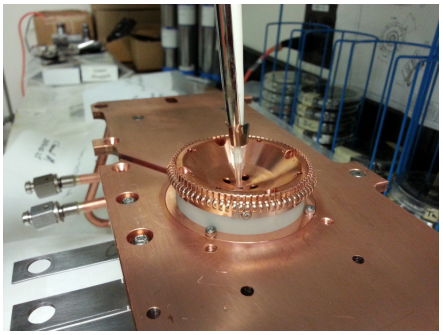

(b) Injecting the salt.

Figure 5.1: Salt injection into the ion transfer tube.

Figure 5.2 shows the receiving coupling plate for the target assembly. The ground electrode can be seen in the middle of the figure.

With the target container in place (fig. 5.3) the vessel was closed and the vacuum pumps were turned on.

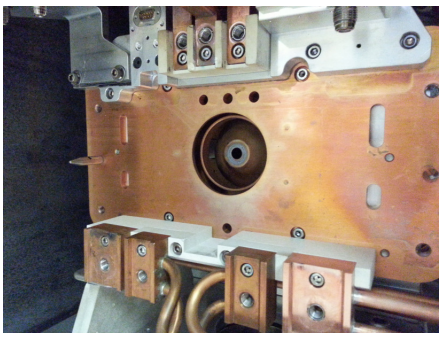

Figure 5.2: Interior of the ISAC test stand to place the ion sources to be characterized.

Once the entire vessel reached a high vacuum environment the ion transfer tube was heated with a DC current of 130 A, which raises the temperature of the ion transfer tube to approximately 2000°C. The nominal high voltage of 30 kV was set to the target assembly. A mass spectrometry analysis was performed to verify the intensity of the ions present in the beam. This is accomplished by letting the particles pass through a tunable magnetic field generated with a dipole magnet. As the magnetic field varies the particles deflects depending on their mass-to-charge-ratio.

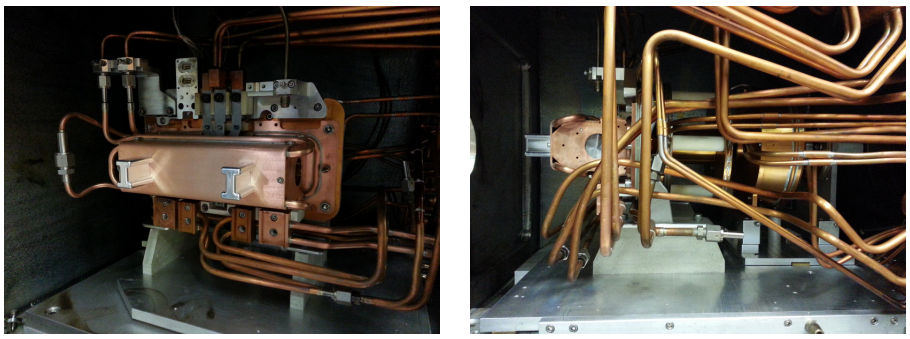

(a) Front view (b) Side view

Figure 5.3: Target assembly put in place for tests. (a) Front view where the ion transfer tube is inside the copper assembly. (b) Side view where the target assembly is located to the left of the image.

The analysis corroborates the mixture of salts used for the test, as it peaks on masses 7, 23, 39, 85 and 132.

Preliminary measurements were conducted to learn the use of optic elements in the beamline as well as the procedure to measure both the emittance and beam profile. Once the ions evaporated completely, the target assembly was removed and the ion transfer tube was refilled with the salt mixture of table 5.2, this based on the good signal provided by those species, however rubidium is the species selected to measure beam properties. Due to the fact that the ion transfer tube used for the experiment did not have an end wall, more volume of the salts would have only caused a backflow of the ions. This means, that some ions would have escaped through the back of the tube and hence the signal would have not increased (A. Mjøs, personal communication, 2016).

Table 5.2: Values use in the mixture of salts for final tests.

Element	Volume [μL]	Mass (amu)
Li	0	7
Na	0	23
K	10	39
Rb	10	85
Cs	5	132

5.1 Default geometry

The geometry corresponds to that of figure 2.1, having three electrodes: the plasma electrode, the extraction electrode and the ground electrode

The extraction electrode (fig. 5.4) was set to the voltages considered in the simulations.

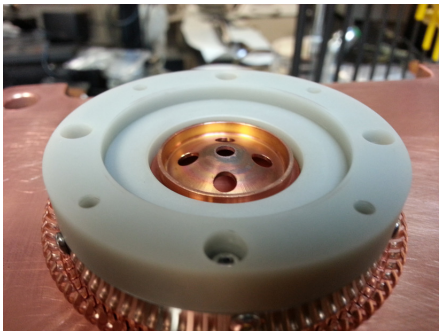

Figure 5.4: Extraction electrode tip (copper). Ceramic insulator (white).

The emittance increases with the extraction voltage as expected from the simulation, as shown in figure 5.5. The error bars from the measurement come from the signal-to-noise-ratio, when low, the error bars are larger.

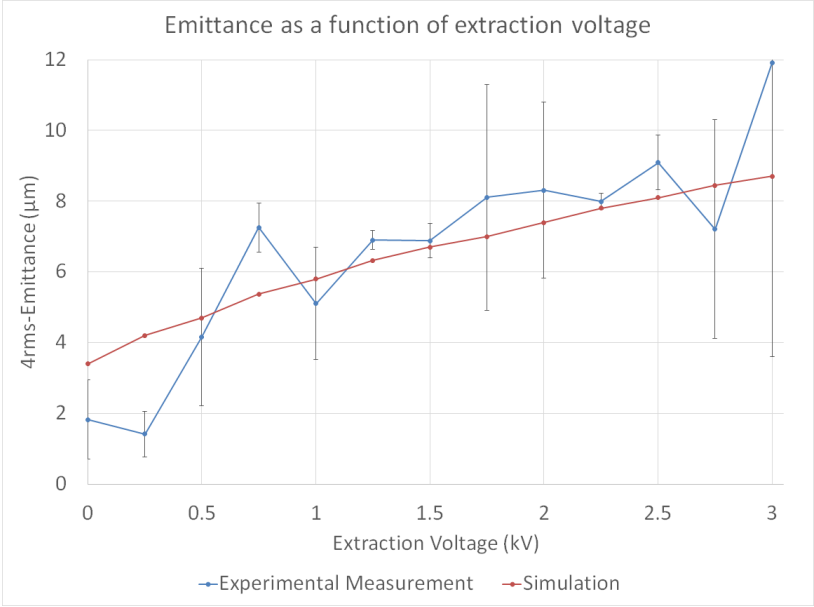

Figure 5.5: Emittance measurements compared to simulation results for ISAC's default geometry.

The beam size presents a minimum around 1 kV and increases on the extremes, that is at 0 kV and 3 kV. The general behavior from the simulation is observed with the experiment (fig. 5.6). An important remark is that the beam size from the simulation was scored at the exit of the ground electrode and the experimental value was measured at almost 2 m downstream from the ground electrode. The behavior, however, remains the same at this distance. By knowing the emittance, the spot size, and the distance, the divergence angle can be found. This value allows to calculate the increase in size of the beam after traveling this distance. The beam size at this far location is found to have 3.5 times the size from the simulation. This value is used to scale the simulation and be able to plot it alongside the experimental value. At higher voltages the simulation is slightly higher than expected, this is most likely because some optic elements were not taken into consideration when estimating the scaling factor.

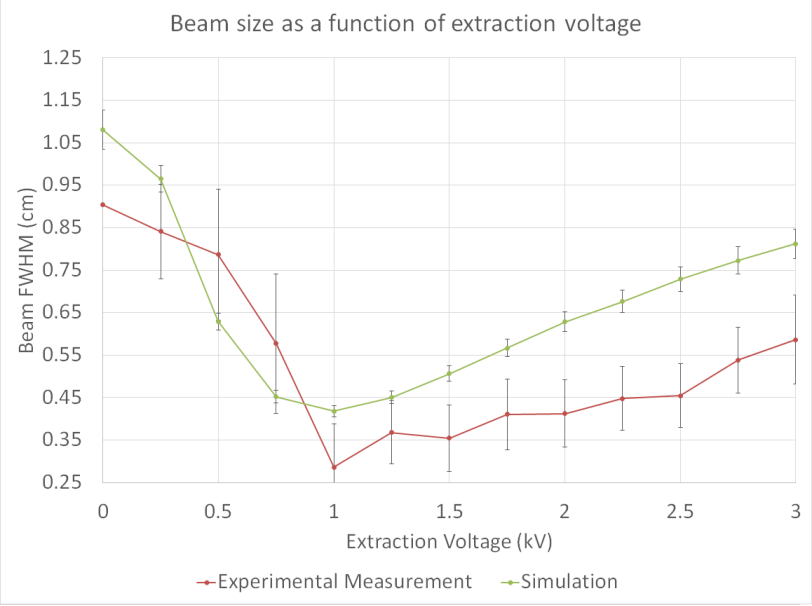

Figure 5.6: Beam size measured and scaled size from simulation for ISAC's default geometry.

The intensity shows an increase with the extraction voltage. The intensity from the simulation was normalized to the maximum value registered in the experiment (fig. 5.7).

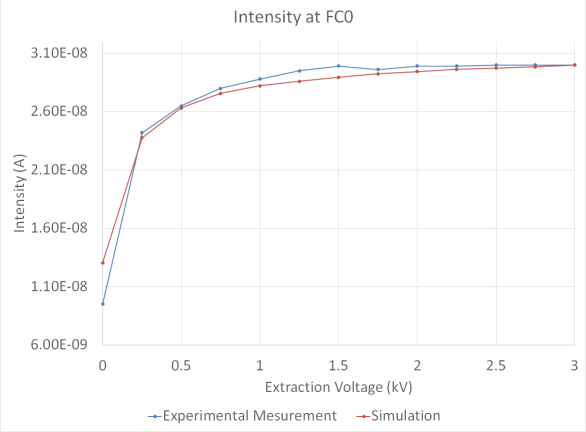

Figure 5.7: Intensity measured and scaled intensity from simulation.

5.2 Removed plasma electrode geometry

The plasma electrode (fig. 5.8) is sandwiched between the ion source and the extraction electrode. It was removed in order to verify its impact on the beam properties. When removed, the ion tube outlet is exposed (fig. 5.8a).

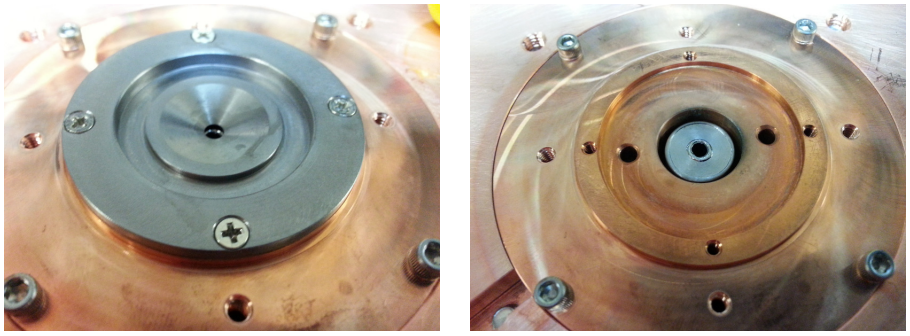

(a) Plasma electrode in place (b) Plasma electrode removed

Figure 5.8: Plasma electrode exposed when refilling the salts.

As before, the emittance increases with the extraction voltage. Figure 5.9 shows good agreement with the simulations.

The beam size is large on the extremes and presents a minimum around 1.5 kV. The simulation shows the same trend but with a minimum around 1 kV (fig. 5.10).

The measured intensity drops when the extraction voltage is raised above 1 kV (fig. 5.11). This could be due to the reservoir being depleted over time. The measurement could not be repeated because of the limitation on time on the test stand.

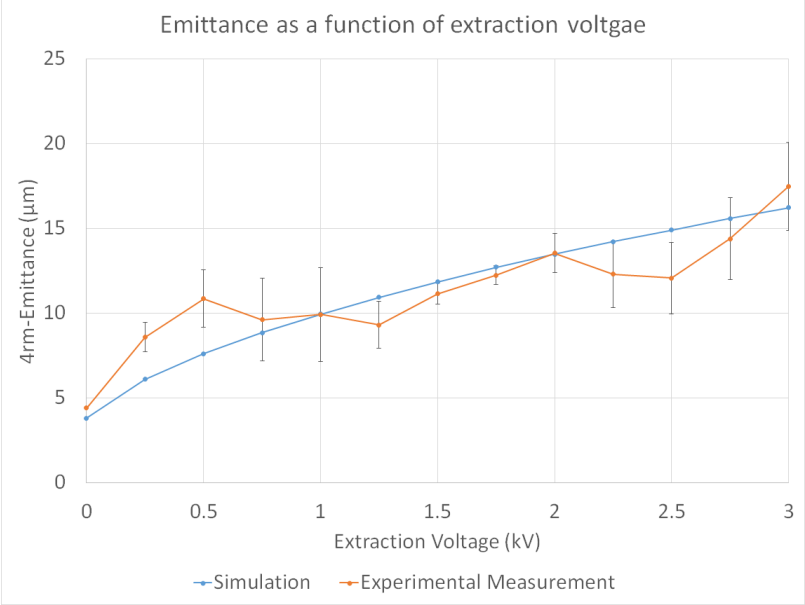

Figure 5.9: Emittance measured and from simulation for ISAC's geometry with the plasma electrode removed.

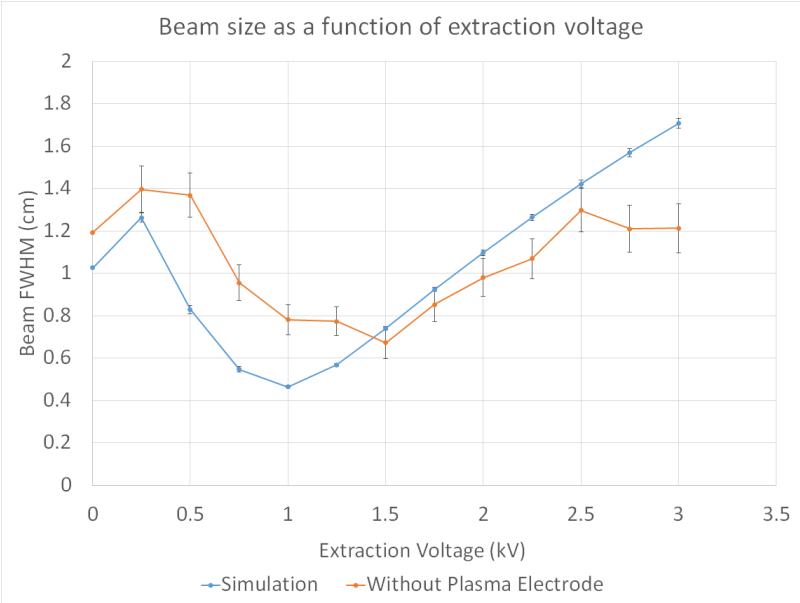

Figure 5.10: Beam size measured and scaled size from simulation for ISAC's geometry with the plasma electrode removed.

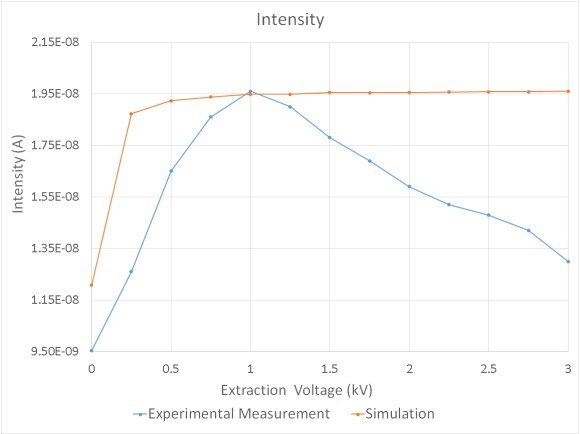

Figure 5.11: Intensity measured and scales intensity from simulation.

5.3 ARIEL-like configurations

The emittance and spot size were measured for the two geometries without the extraction electrode as described in section 4.3, ground electrode only (GO) and ground electrode plus plasma electrode (PG). The values are reported in table 5.3

Table 5.3: Beam parameters measured and from simulation for ARIEL-like configurations.

	Ground only		Plasma plus ground	
	simulation	measured	simulation	measured
$4\epsilon_{\text{rms}}$	21.88 μm	22.11 $\pm$3.8 μm	9.31 μm	9.56 $\pm$ 2.58 μm
Beam size FWHM	1.33 cm (scaled)	1.49 $\pm$0.04 cm	0.87 cm (scaled)	0.90 $\pm$ 0.03 cm

5.4 Discussion

Figure 5.12 compares how the measured emittance grows with the extraction voltage for the two geometries. With the plasma electrode the emittance is significantly smaller for all extraction voltages. The shape of the potential in front of the ion source affects directly the transverse velocity of the particles and this translates into an increased emittance.

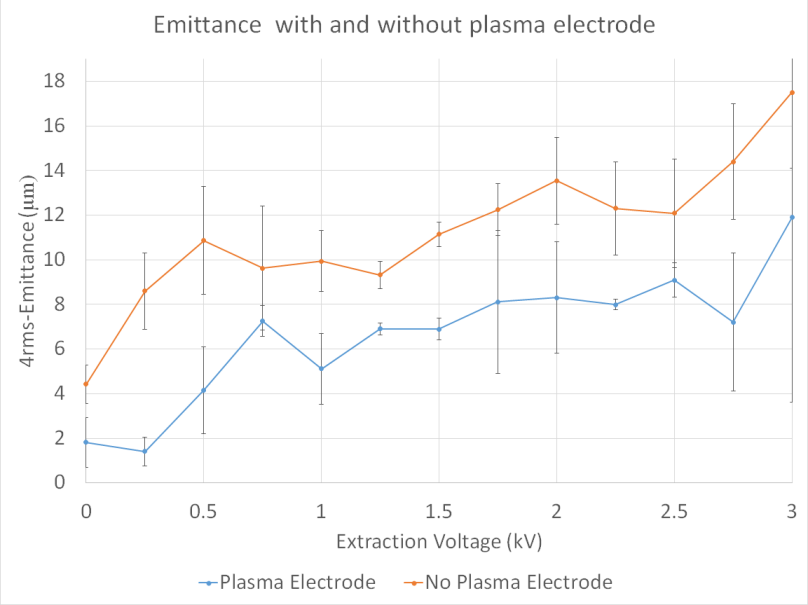

Figure 5.12: Emittance measured for both ISAC's geometry studied cases. With and without plasma electrode.

Figure 5.13 shows both measured spot sizes. The spot size behaves similarly for the two geometries: larger on the extremes and a minimum in between. The minimum for both geometries occurs at similar extraction voltages. The spot size is smaller with the plasma electrode.

The overall methodology for simulations seems accurate and powerful for describing the experimental data.

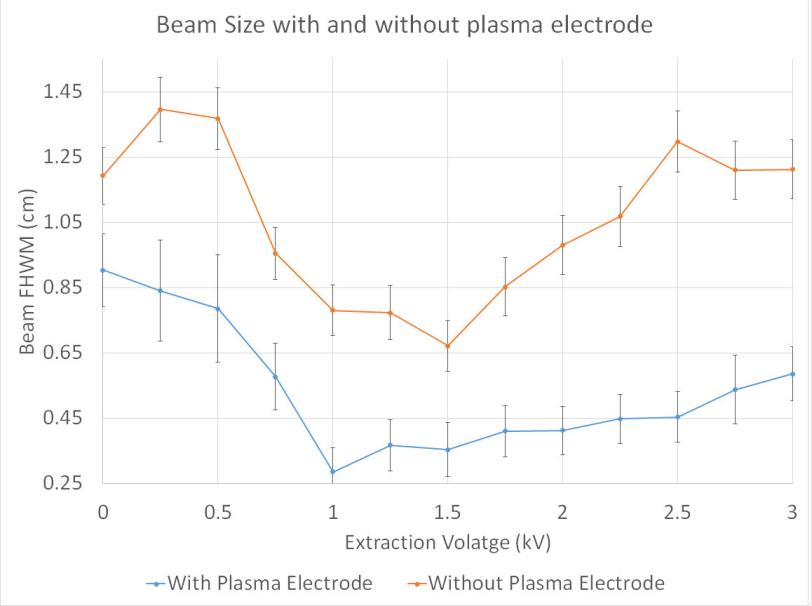

Figure 5.13: Beam size measured for both ISAC's geometry studied cases. With and without plasma electrode.

Chapter 6

ARIEL Ion Optics Simulation Studies

In previous chapters, the ISAC three electrode system was modified to study beam properties in a single electrode configuration and these were investigated experimentally and through simulations. This was done in order to have similar but non optimized conditions as in the ARIEL configuration and therefore to validate the simulation methodology. The new design shall allow more flexibility in the choice of ion souces and will mitigate the problems with short cuts between the tube and the extraction electrode plus avoid potential losses at the plasma electrode. The proposed geometry for ARIEL consists of a smaller single electrode set to ground similar to the configuration used at the ISOLDE facility at CERN [11]. It includes a tubular section that serves as a mounting feature that allows the electrode to be moved based on the space and beam requirements of the ion sources being used. The proposed design for the ARIEL ion optics extraction system needs to be optimized in order to be able to transport all the ions without losses to guarantee the maximum intensities of the RIBs, with a minimum spot size and emittance, which is the focus of this chapter.

The main geometry was drawn in Solidworks (fig. 6.1). There are two main units in the system: the chamber and the extraction electrode. The chamber provides a vacuum environment and is set to different voltages in different sections as will be shown later on. The center of the downstream end of the ion transfer tube is used as the origin of a coordinate system $x-y$ perpendicular to the traveling direction of the particles, z. Figure 6.1 shows an isometric view of the extraction electrode alongside with a cut view of the chamber. The length of the electrode tubular section is fixed to

300 mm. The length of the downstram chamber is still in design and for the studies carried out in this chapter it will be fixed to 1200 mm.

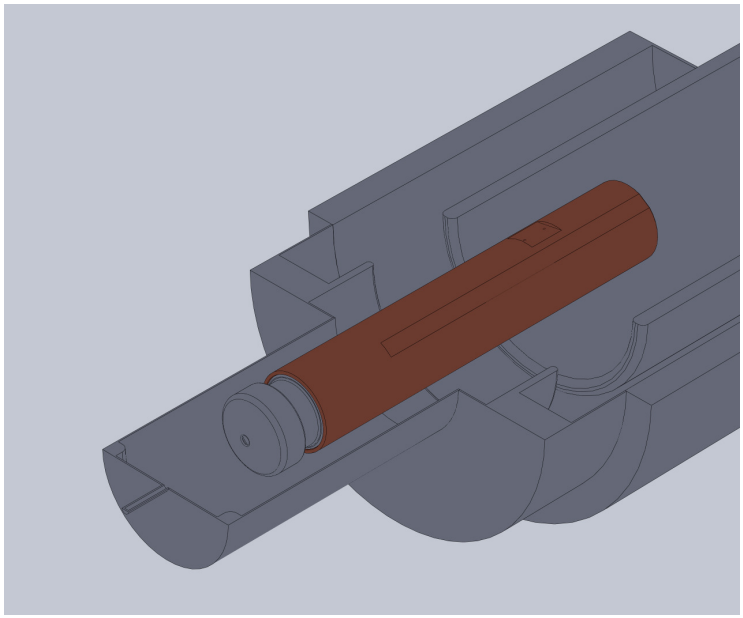

Figure 6.1: Semi-cut of the isometric view of the chamber with the extraction electrode.

The exchangeable tip of the extraction electrode is shown in figure 6.2. The main purpose of the tip is to shape the electric potential inside the chamber.

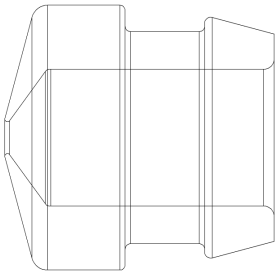

Figure 6.2: Schematic drawing of the extraction electrode tip.

Simulations were performed in Comsol for 3000 particles of mass 98 amu generated in the interior of the ion source tube. The high voltage of the system was set to the nominal value of 60 kV.

All properties are taken at z=1200 mm, unless otherwise stated.

6.1 Acceleration gap

The very first step towards the optimal design was to find a suitable distance between the ion source and the tip of the extraction electrode. Even though there are some physics restrictions for having the ion transfer tube and the electrode too close, for example to avoid excessive field strength, all cases were simulated in order to see the behavior of the beam parameters over a large range of values (table 6.1).

Table 6.1: Range of values considered for the acceleration gap.

Parameter	Values	Comment
Acceleration gap	10-200 mm	steps of 10 mm

Figure 6.3 shows the electric potential for selected values of acceleration gap. The main feature to observe in these images is the potential at the exit of the ion transfer tube where the electric field increases when the gap is smaller.

Moreover, figure 6.4 shows the electric equipotential lines at the outlet of the ion transfer tube for gap=40 mm. This image also includes a grid of the electric field vectors and the large diagonal fields near (z,x)=(0,±1.5) mm would cause a large acceleration of the ions into an undesired trajectory.

Particles were generated within the interior of the ion transfer tube and the trajectories were computed. The trajectories are shown in figure 6.5, where the particles travel from left to right. The beam size at the end of the chamber—far right, changes in size when the electrode is displaced.

The corresponding beam profiles are shown in figure 6.6. For the cases shown, gap=60 mm, shows the most narrow profile.

On the zoom of the particle trajectory (fig. 6.7) some ions are seen to hit the tip of extraction electrode which significantly reduces the efficiency of the system. The color scale indicate kinetic energy in keV.

The dependence of the emittance on the acceleration gap is shown in figure 6.8. The emittance decreases with a larger gap and the transmission efficiency reaches 100% after 80 mm. Figure 6.9 shows the dependence of the beam size on the acceleration gap and exhibits a minimum at gap= 70 mm.

The phase space is shown in figure 6.10. The beam diverges more in 6.10a, as can be seen in the vertical axis, this translate to the large beam size as can be seen in

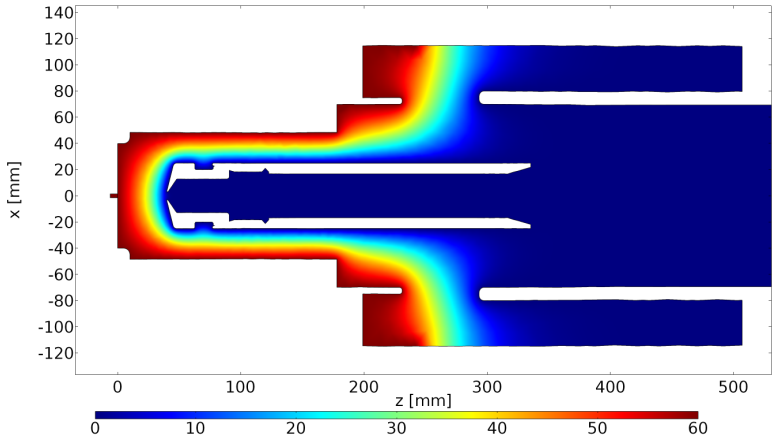

(a) gap =40 mm

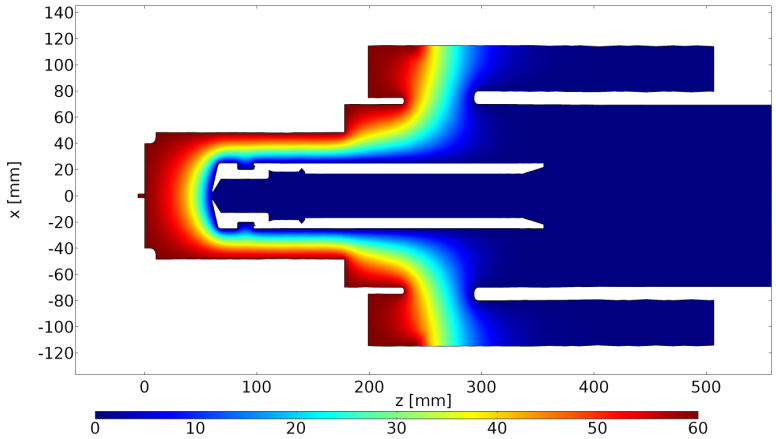

(b) gap =60 mm

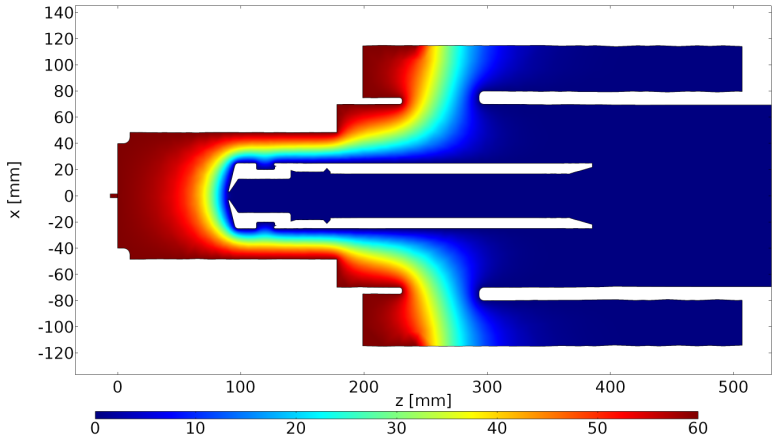

(c) gap = 90 mm

Figure 6.3: Electric potential at different gaps. The color scale is in kV.

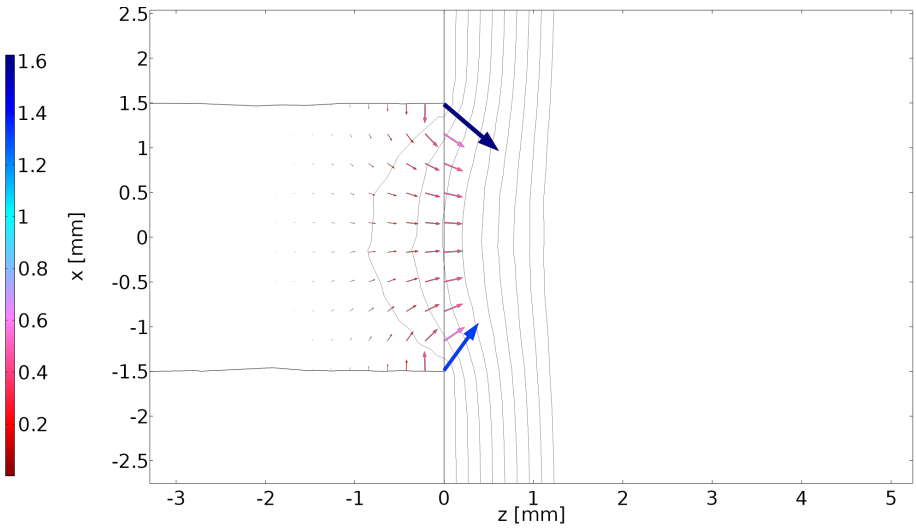

Figure 6.4: Electric field and equipotential lines at 40 mm. The color scale indicates the electric field strength in kV/mm.

the horizontal axis. For gap = 60 mm, figure 6.10b shows a smaller beam size and divergence compared to 6.10a and 6.10c.

6.2 Outlet angle

Given the fact that some losses are present in the design described in the previous section, the shape of the exit of the ion transfer tube was adjusted in order to minimize the losses or avoid them completely. Instead of adding a separated electrode, as in ISAC, a built-in angle is added to the surface of the chamber, as shown in figure 6.11. The base of the triangle formed with the horizontal line and the angle is fixed to 5 mm in order to fully defined the acceleration gap, which is fixed at the nominal value, 60 mm. An angle of 0° would create an extension of the transfer tube and the effective acceleration gap distance would not be defined in the same way as in previous section. The previous section would correspond to an angle of 90°. The values studied are given in table 6.2.

Table 6.2: Range of values considered for the outlet angle.

Parameter	Values	Comment
Outlet Angle	15-75°	steps of 15°

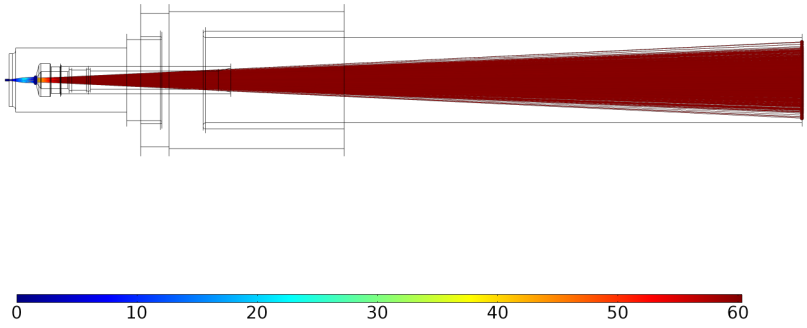

(a) gap =40 mm

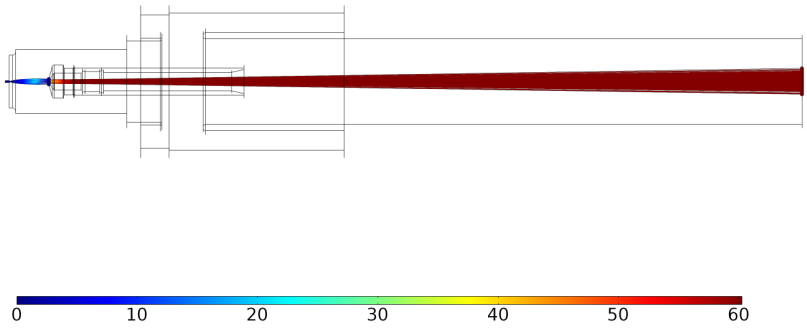

(b) gap =60 mm

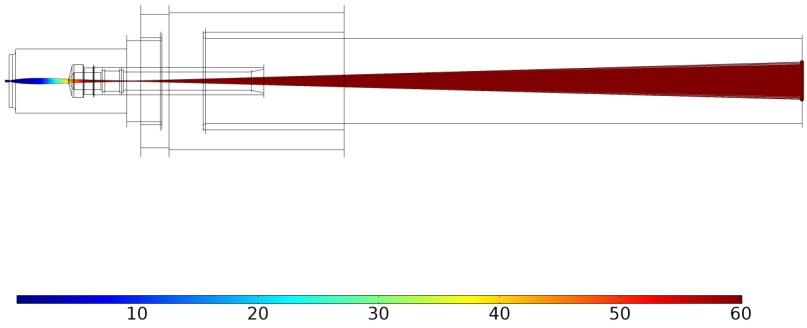

(c) gap = 90 mm

Figure 6.5: Particle trajectory for different gaps. The color scale indicates the particle kinetic energy in keV.

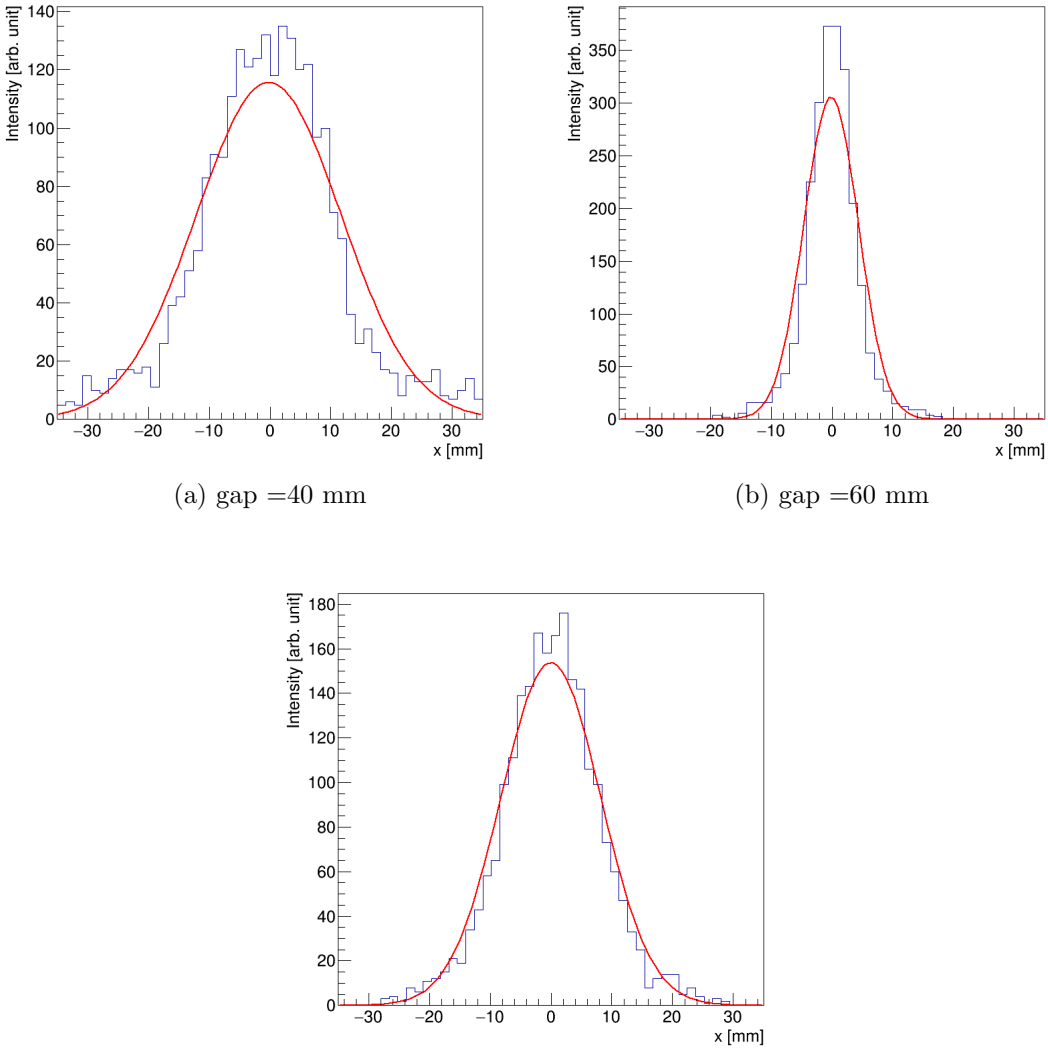

(a) gap =40 mm

(b) gap =60 mm

(c) gap = 90 mm

Figure 6.6: Beam profile for different acceleration gaps. The red line is the best fit to the data.

The electric potential for chosen angles of this configuration can be seen on figure 6.12.

Figure 6.13 shows the particle trajectories and it is seen that there are no losses for an angle=45° but there are some for angle=75°.

The emittance increases with the outlet angle, as shown in figure 6.14. Here it is seen that the transmission efficiency is 100% from 30° to 60° and then decreases with a larger angle.

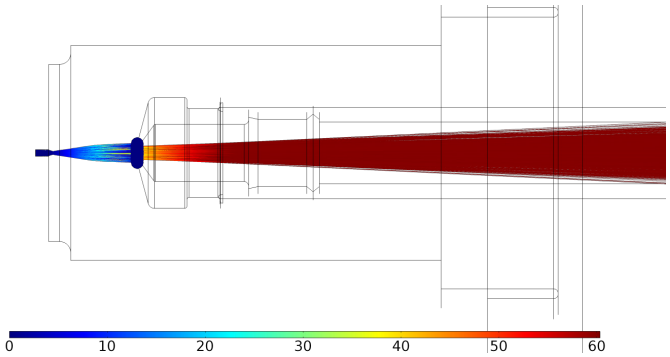

(a) gap =40 mm

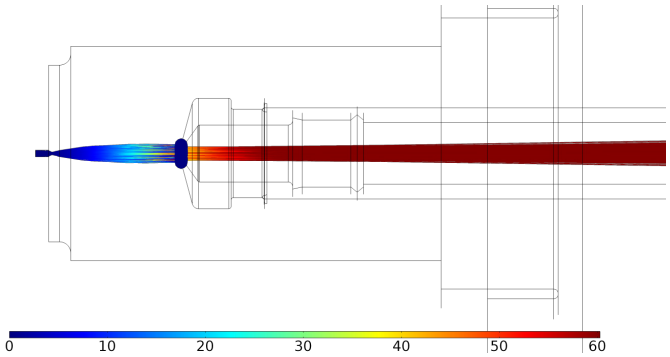

(b) gap =60 mm

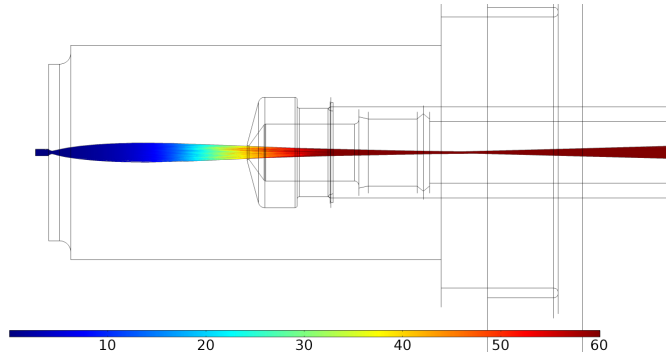

(c) gap = 90 mm

Figure 6.7: Particle trajectory detail at different gaps

Figure 6.15 shows a similar behavior of the beam size to that of section 4.4. Larger at the extremes and a minimum occurs around 60°.

The phase space is shown in figure 6.16. It shows two similar distributions, however, figure 6.16b presents some tails extending out of the center. These tails correspond to some particles out of the main core of the beam, and comes from the particles generated near the exit of the transfer tube that receives a larger velocity due to the higher electric field.

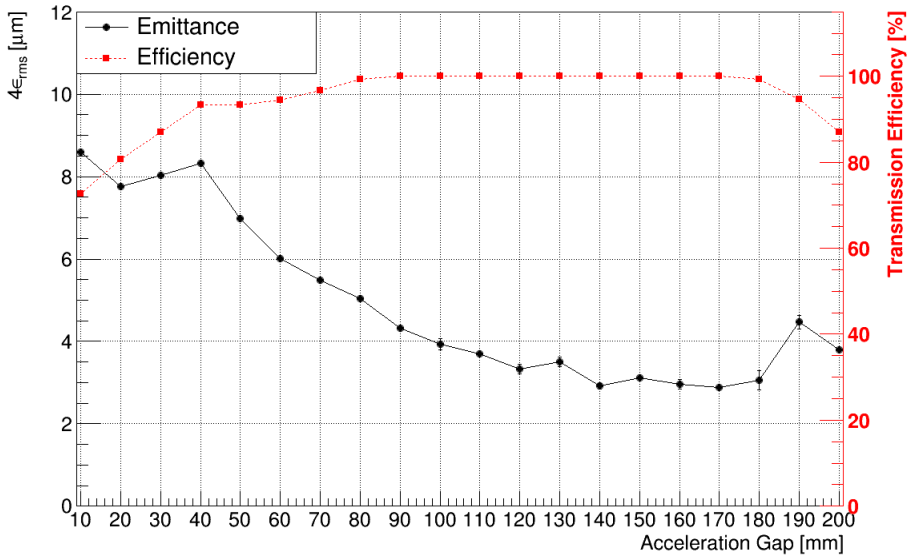

Figure 6.8: Beam emittance and transmission efficiency as a function of acceleration gap.

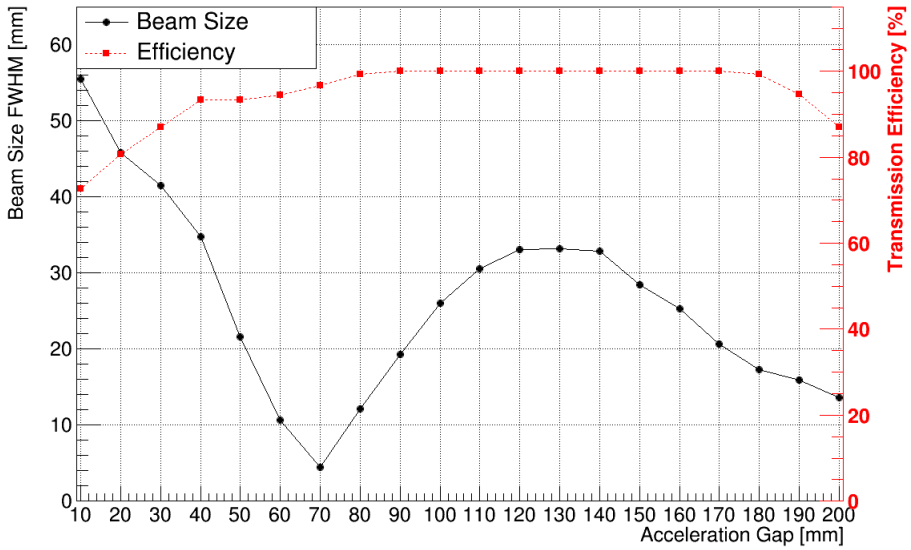

Figure 6.9: Beam size and transmission efficiency as a function of acceleration gap.

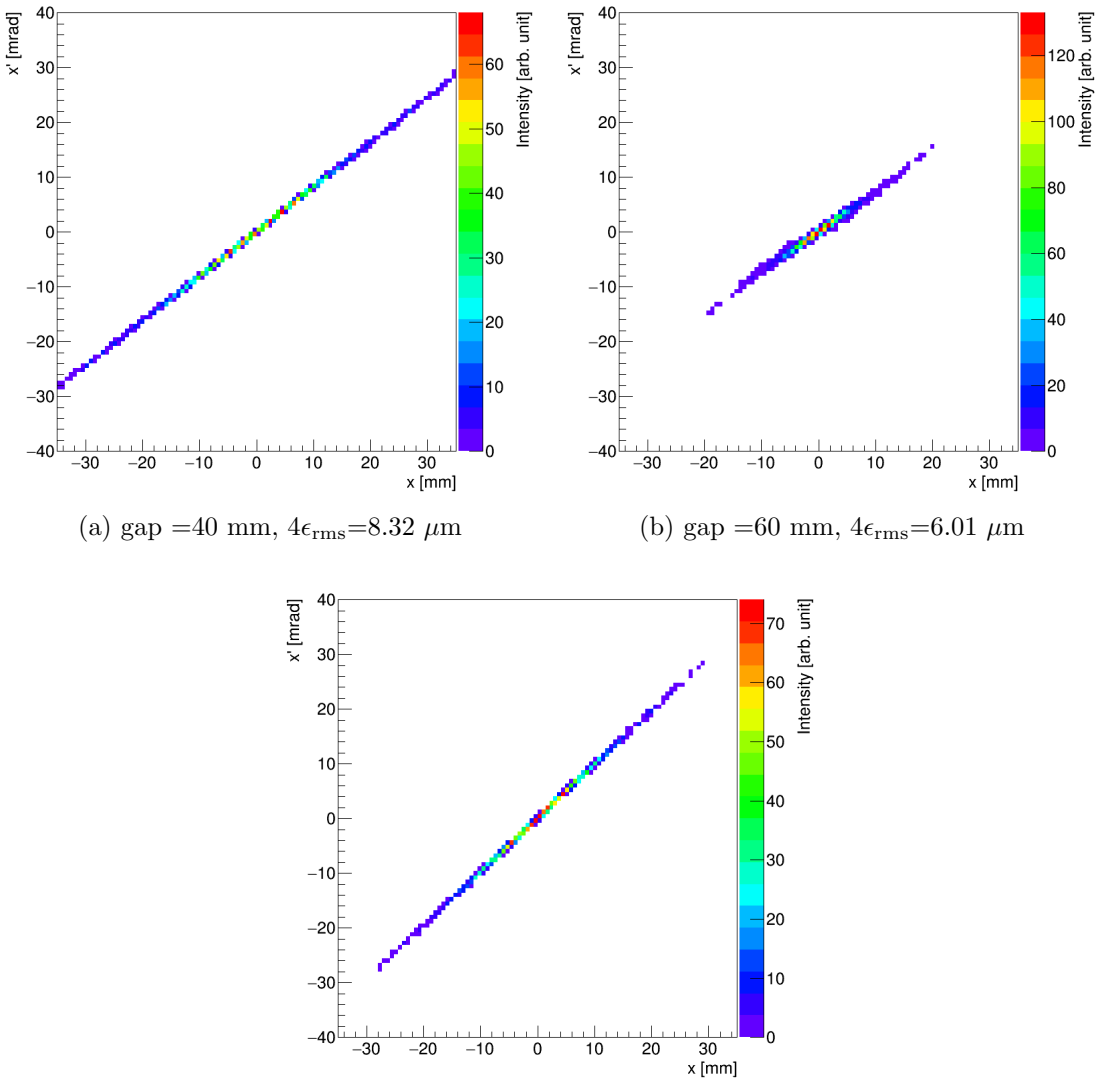

(a) gap =40 mm, $4\epsilon_{\text{rms}}$=8.32 μm

(b) gap =60 mm, $4\epsilon_{\text{rms}}$=6.01 μm

(c) gap = 90 mm, $4\epsilon_{\text{rms}}$=4.32 μm

Figure 6.10: Emittance for different acceleration gaps.

6.3 Acceleration gap with optimized outlet angle

Based on the results of the outlet angle sweep, an angle of 60° is set as the optimized geometry. In this section, the behavior of the acceleration gap in this new configuration is verified for gaps of 60, 70 and 80 mm.

The emittance (fig. 6.17) shows the same behavior as before, decreasing with a larger gap, however, with lower values and now 100% efficiency is achieved at 60 mm.

The phase space is shown in figure 6.18.

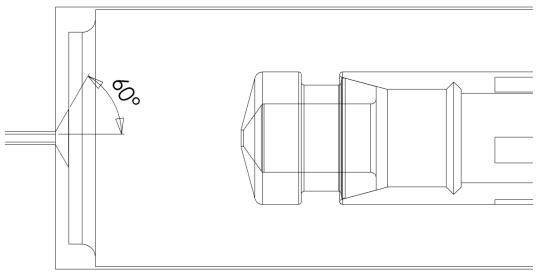

Figure 6.11: Schematic drawing of the outlet angle.

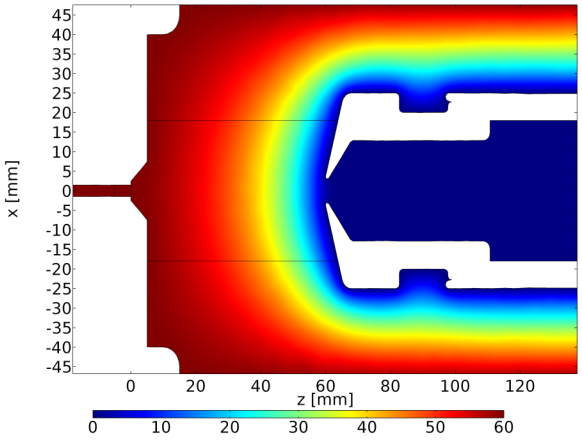

(a) angle =45°

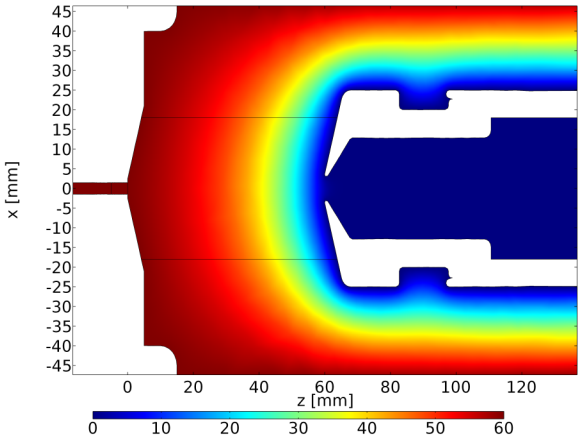

(b) angle =75°

Figure 6.12: Electric potential for different outlet angles. The color scale is in kV.

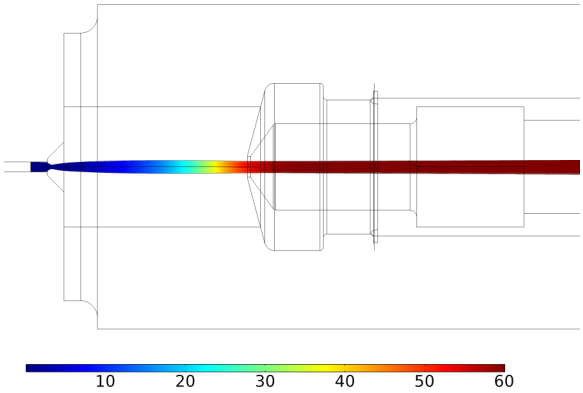

(a) angle =45°

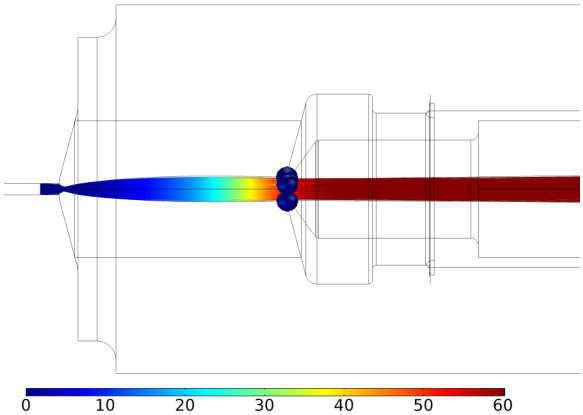

(b) angle =75°

Figure 6.13: Particle trajectory detail for different outlet angles at the nominal gap of 60 mm.

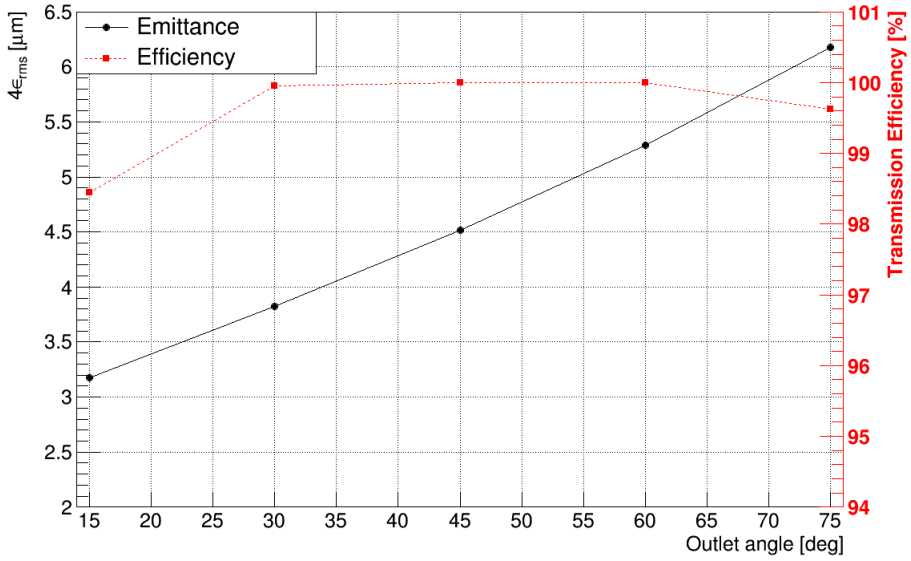

Figure 6.14: Beam emittance and transmission efficiency as a function of outlet angle

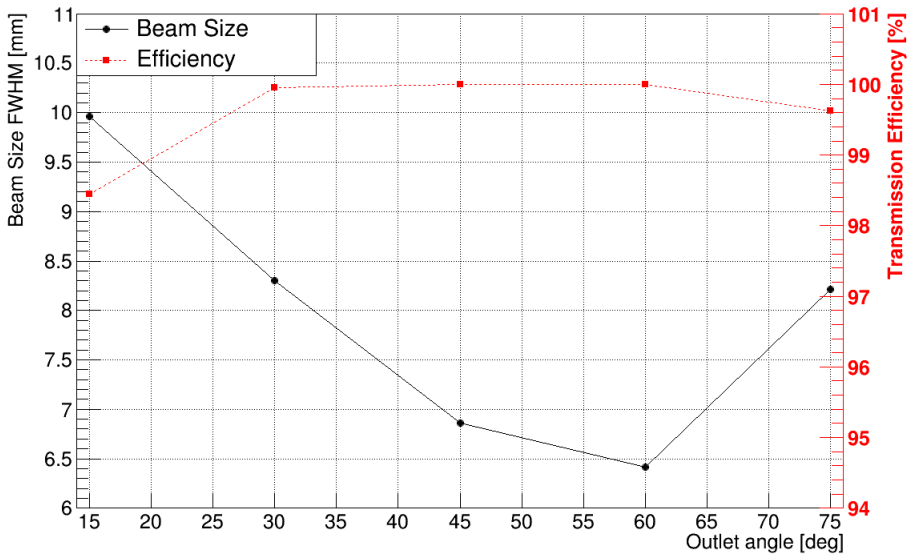

Figure 6.15: Beam size and Transmission efficiency as a function of outlet angle

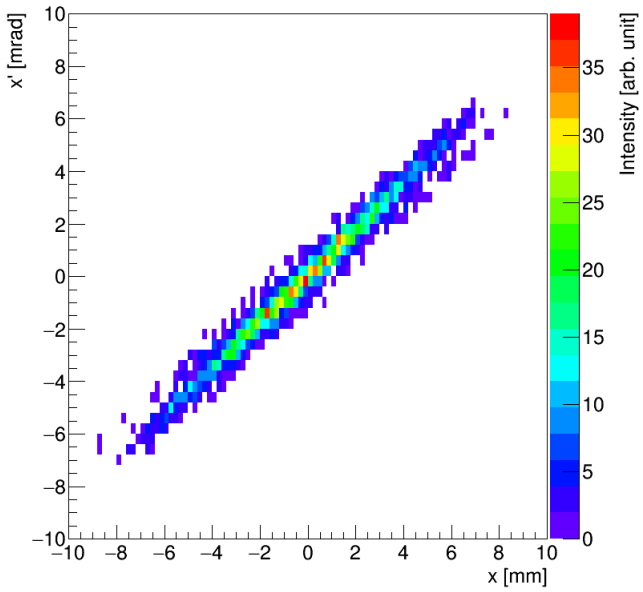

(a) angle =45°, $4\epsilon_{\mathrm{rms}}$= 4.51 μm

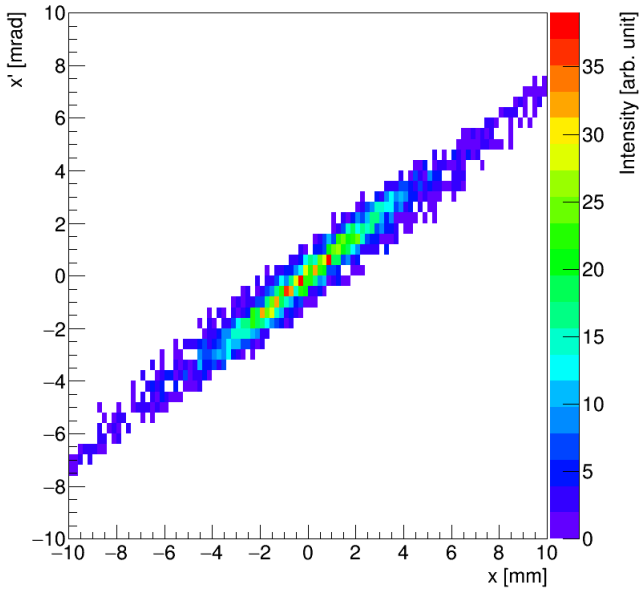

(b) angle =75°, $4\epsilon_{\mathrm{rms}}$= 6.18 μm

Figure 6.16: Phase space at different outlet angles.

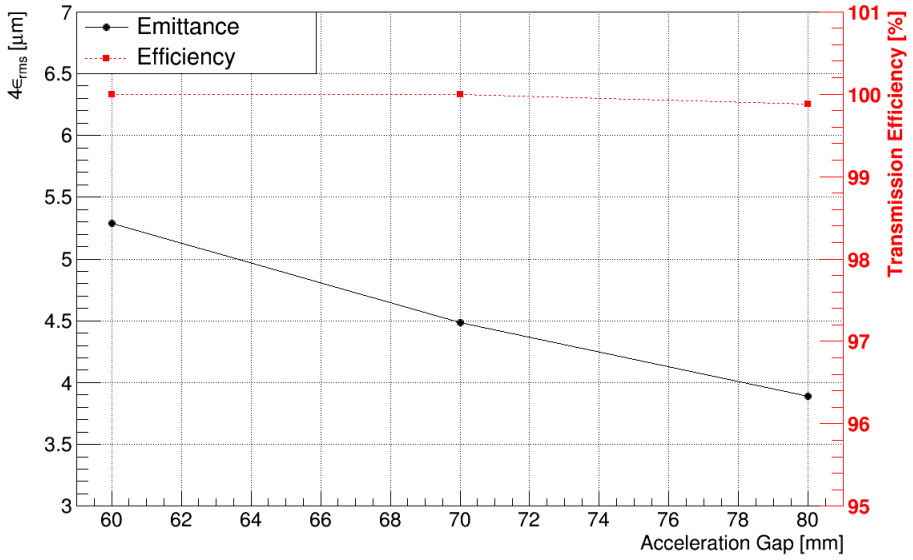

Figure 6.17: Beam emittance and transmission efficiency as a function of acceleration gap for optimized outlet angle.

On the other hand, in figure 6.19, the beam size shows a small value at 70 mm. Given the fact that at this point there is a 100% efficiency and the elliptical shape of the phase space is desirable for better beam transportation, this value will be set as the default geometry alongside with the outlet angle of 60°.

For this "new" default geometry (table 6.20) , an additional analysis is performed on how the beam envelope scales when traveling from the ion transfer tube to the end of the chamber (fig 6.20). The beam size is shown as vertical bars and presents a minimum around 200 mm, inside the ground electrode tube.

The beam profile at the end of the chamber is shown to be gaussian in figure 6.21.

6.4 High voltage

Based on the improved default geometry (table 6.3), a verification of the correct functionality at lower voltages was studied. This is needed to match the RIB requirements for some experiments [3].

The voltages used for this study are shown in table 6.4. The emittance and beam size as function of voltage, figures 6.22 and 6.23 respectively, show a decrease when the high voltage is increased. The transmission efficiency is 100% for all cases.

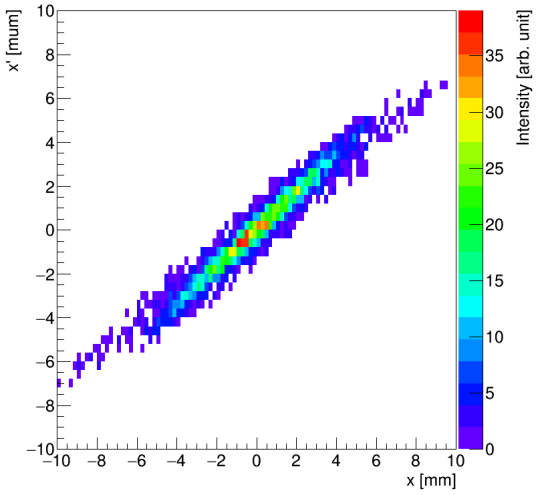

(a) gap =60 mm

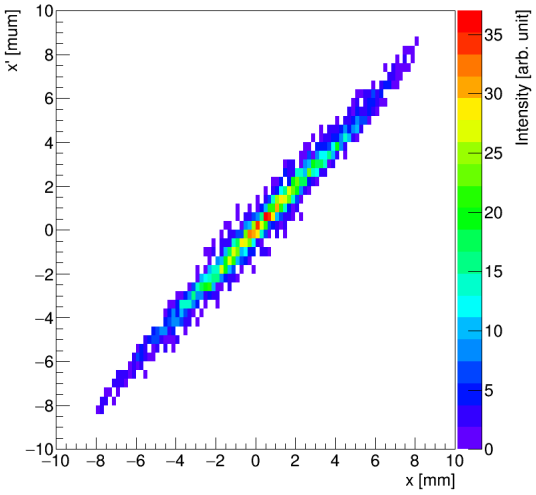

(b) gap =70 mm

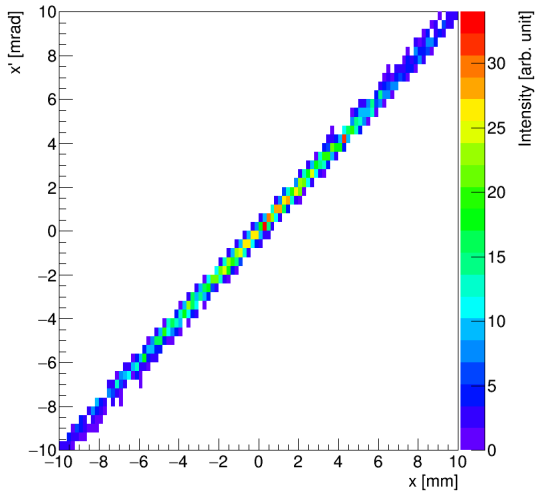

(c) gap = 80 mm

Figure 6.18: Phase space at different gaps for the optimized outlet angle.

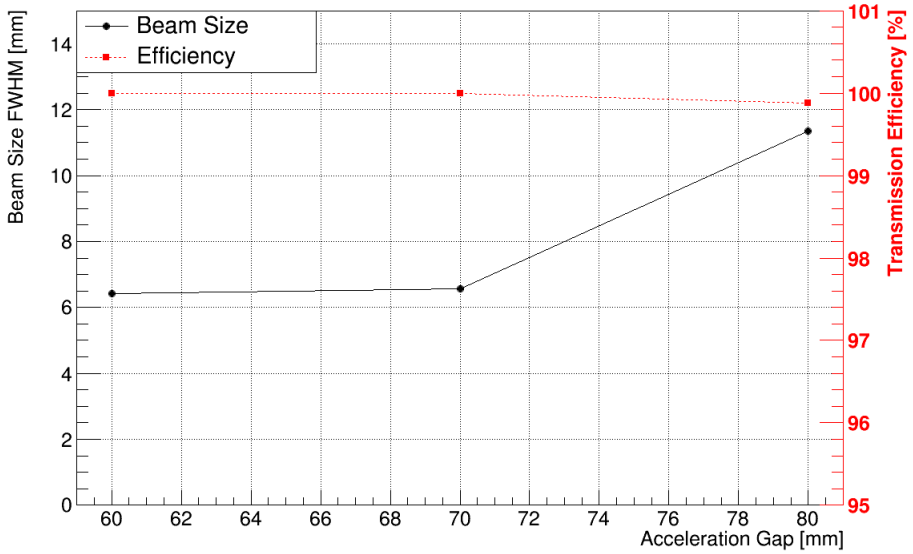

Figure 6.19: Beam size and transmission efficiency as a function of acceleration gap for optimized outlet angle.

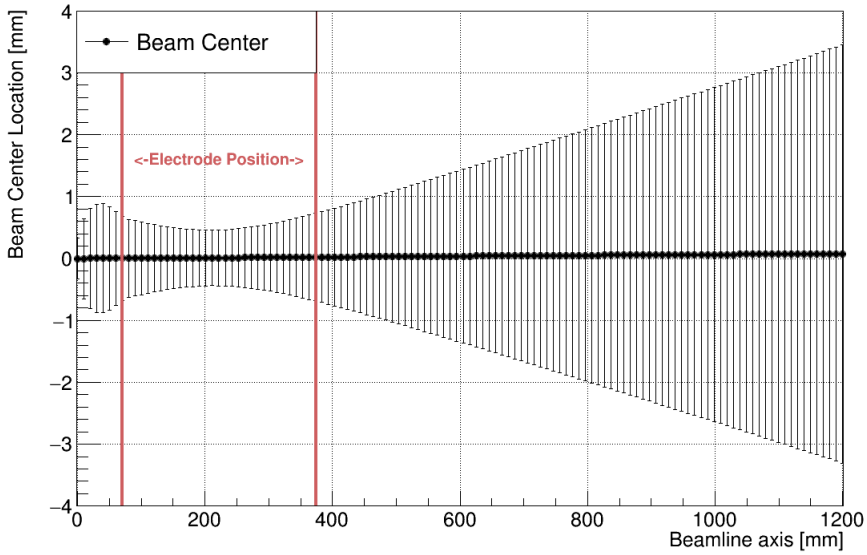

Figure 6.20: Beam size alongside the position in the beamline.

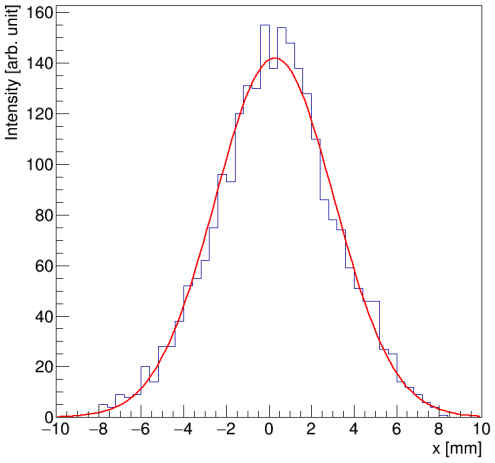

Figure 6.21: Beam profile at the end of beamline. The red line is best fit to the data.

Table 6.3: Improved default geometry.

Parameter	Value
Acceleration gap	70 mm
Outlet angle	60°
4-emittance	4.4 μm
Beam size FWHM	6.4 mm

Table 6.4: Range of voltages considered.

Parameter	Values	Comment
Extraction Voltage	10-70 kV	steps of 10 kV

6.5 Ion mass

Another study performed on the improved default geometry (table 6.3) was to verify that the different species produced can be transported. The masses swept are in table 6.5 and represents the typical range of ARIEL beams.

Table 6.5: Range of masses considered.

Parameter	Values	Comment
Ion Mass	1-300 amu	steps of 1 amu

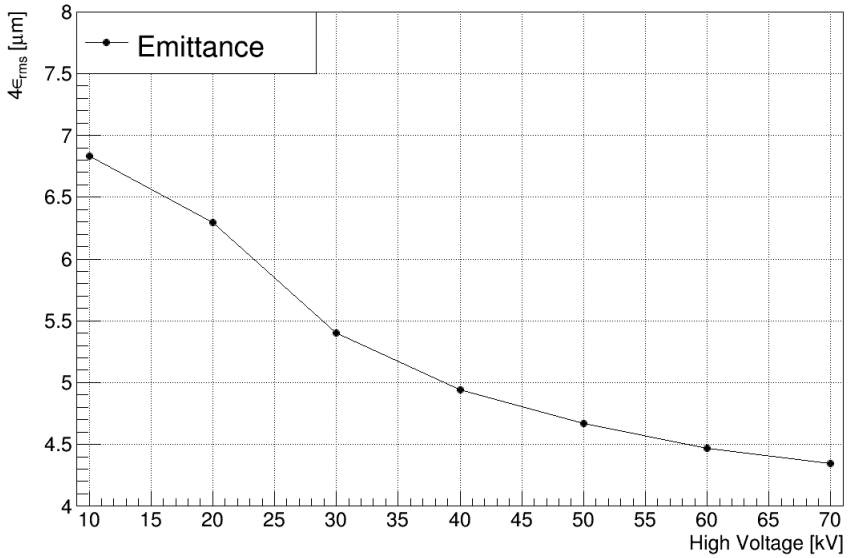

Figure 6.22: Beam emittance and transmission efficiency as a function of extraction voltage for optimized geometry.

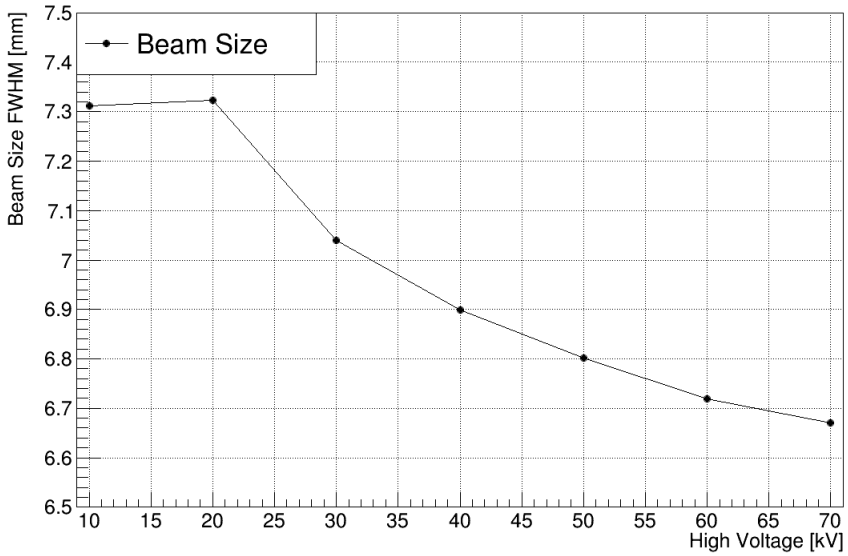

Figure 6.23: Beam size and transmission efficiency as a function of extraction voltage for optimized geometry.

The beam emittance and beam size are found to not depend on the ion mass over the range of variation as expected.

6.6 Ion tube source offset

The ion source is put off-center in order to quantify the displacement of the beam at the downstream end of the chamber in the case of a misalignment when placing a new target assembly. It is moved from the origin to $x = -1$ mm (fig. 6.24). The other two coordinates remain unchanged.

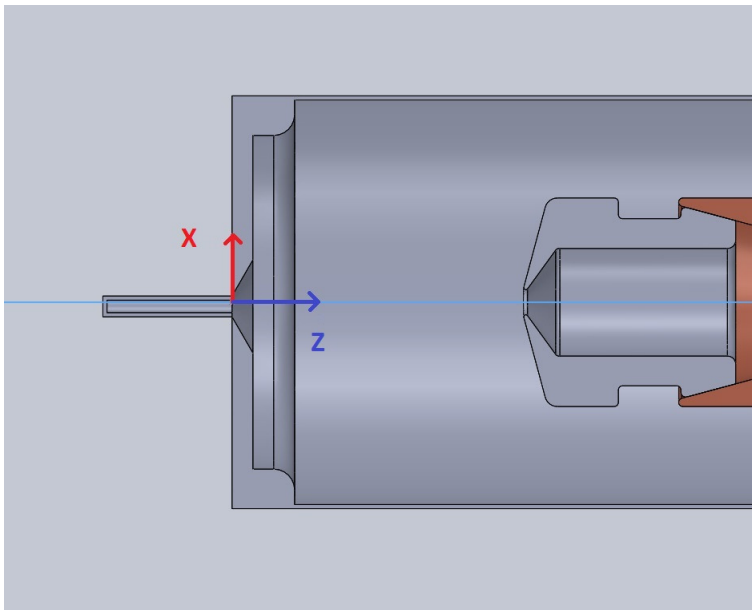

Figure 6.24: Ion transfer tube below the origin. The blue line indicates the center of the system.

The beam offset at the downstream end of the chamber (fig. 6.25) is approximately 0.2 mm. The angle in which the particle travel is undesirable for the following stage of the beam transport system that requires the beam in a straight direction.

A set of steerers is added to counteract the displacement and deflect the beam back on axis. The steerer consists of two parallel plates held to certain potential difference. The proposed size of the plates is set to 50 mm $\times$50 mm separated by a distance of 50 mm. Two sets of steeres are needed to correct the displacement and angle of the beam in one direction. The first steerer is at 460 mm downstream of the ion transfer tube exit, this distance is chosen so that the ground electrode can be displaced if needed. The second steerer is 170 mm downstream of the end of the first steerer.

The position of the beam at the entrance of the first steerer is known from simulations. Equation 6.1 is used to estimate the value of the potential difference needed.

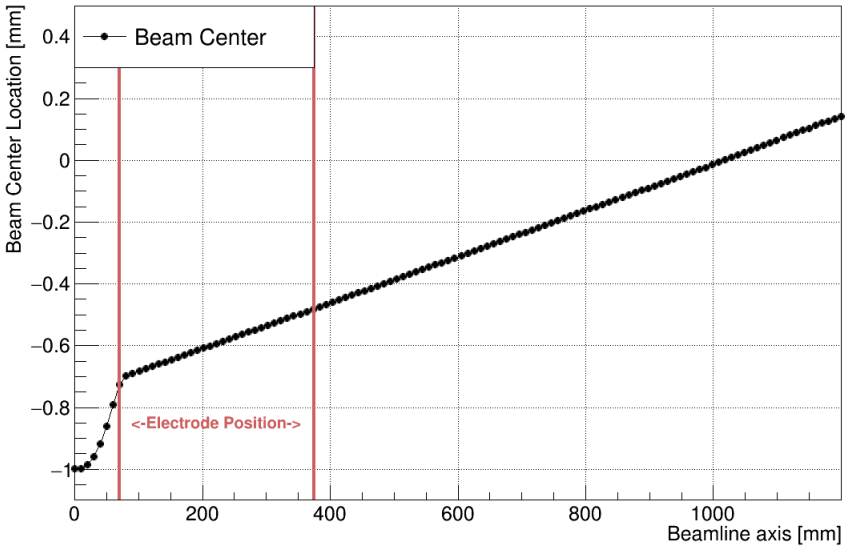

Figure 6.25: Beam center location on the beamline.

$$\theta = \frac{V_{st1}}{V_{source}} \frac{L}{2D} \tag{6.1}$$

Here, V_{st1} is the voltage difference of the steerer, V_{source} is the voltage of the ion source, 60 kV. L is the length of the plate and D is the separation between the plates. Finally, θ is the angle that needs to be corrected.

Figure 6.26, shows the electric field map alongside the electric potential for the steerers. For a 60 keV beam, the voltage difference for the first steerer was found to be 70 V, this difference is obtained, for example, by setting the lower plate to 570 V and the top plate to 500 V. The voltage difference for the second set was found to be 145 V and, for instance, setting the bottom plate to 500 V and the top plate to 645 V fulfill the condition. The voltages are set asymmetrically for the case when the beam is offset in the opposite direction, in this scenario one plate is reduced and the other is increase changing the direction of the electric field. The first steerer kicks the beam towards the center and the second steerer kicks the beam downwards enough to make it travel along the intended direction.

Figure 6.27 shows how the beam can be relocated back again on axis once the steerers are added.

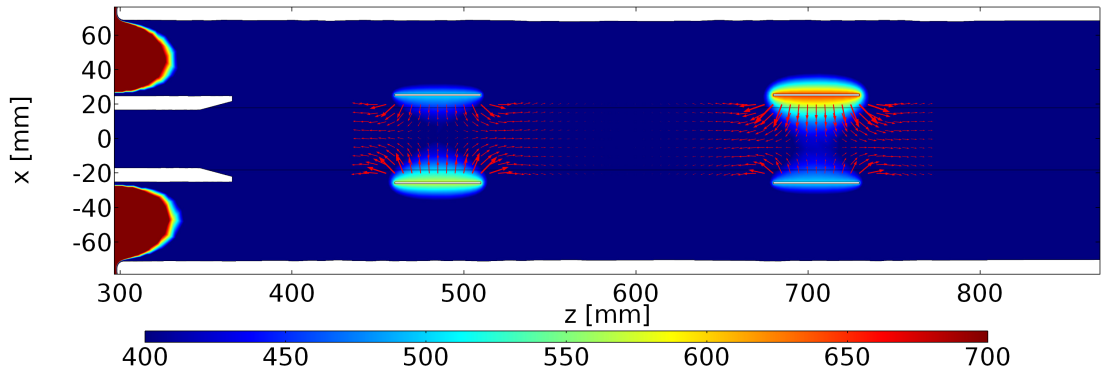

Figure 6.26: Electric field and potential for both steerers. The downstream end of the ground electrode is seen to the left. The color scale indicates the electric potential in V.

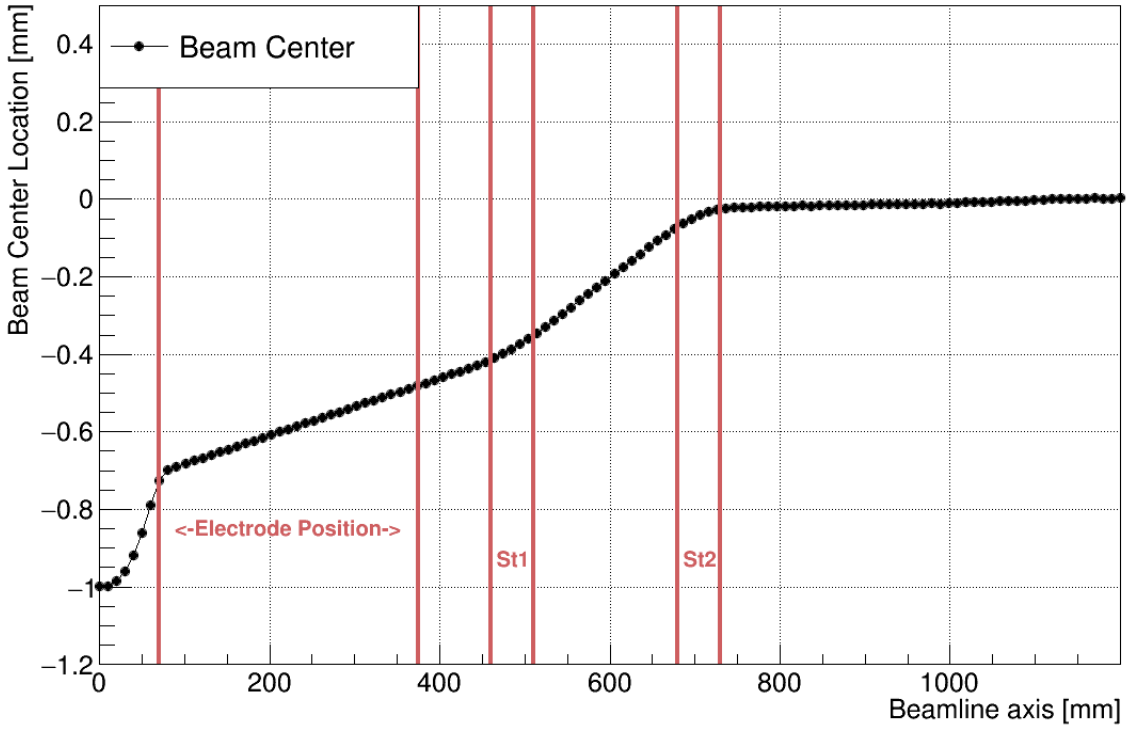

Figure 6.27: Beam center position correction.

Due to the cylindrical symmetry of the system, an offset from the origin to $y = 1$ mm is corrected adding a set of steerers with the same voltage differences but rotated 90°. Finally, the steering is found to not affect the beam size nor the emittance.

Chapter 7

Conclusions

Simulations were performed for a variety of configurations of the ISAC geometry and these were measured experimentally. Basic predictions of the beam properties were verified. It was found that the plasma electrode for ISAC improves beam properties in the particular ISAC case.

To characterize and optimize the proposed ARIEL ion optics design, simulations were performed for a surface ion source. The emittance decreased with the increasing of the acceleration gap and the beam size presented a minimum around 70 mm. Losses on the electrode were observed at this distance and they were cured with the addition of an angle equal to 60 degrees to the outlet of ion transfer tube. The emittance value was found to be 4.4 μm, which is comparable, if not better, to ISAC's performance. The optimized geometry can be used at low voltages without losses. Additionally, a set of steerers accomplished the correction of the beam direction within the space restrictions for 1 mm offset of the ions source.

Finally, Comsol and Solidworks combined provided an excellent tool to estimate the beam parameter for ISAC and ARIEL after identifying a suitable methodology. This combination can provide further analysis on new designs of chambers, ion sources and/or extraction electrodes.

Bibliography

[1] Comsol multiphysics. https://www.comsol.com/.

[2] Solidworks 3d cad. http://www.solidworks.com/.

[3] F. Ames. ARIEL ion sources and ion beam extraction optics requirements specifications. TRIUMF Document-123341, 2015.

[4] F. Ames, P. Bricault, H. Heggen, P. Kunz, J. Lassen, A. Mjøs, S. Raeder, and A. Teigelhfer. Ion source developments for the production of radioactive isotope beams at TRIUMF. *Review of Scientific Instruments*, 85, 2014.

[5] I. Brown. *The Physics and Technology of Ion sources*. Wiley-Interscience, 1989.

[6] R. Brun and F. Rademakers. ROOT - An Object Oriented Data Analysis Framework. In *Proceedings AIHENP'96 Workshop*. Nucl. Inst. & Meth. in Phys. Res. A, 1996.

[7] M. Dombsky, R. Baartman, J. Doornbos, T. Hodges, K. Jayamanna, R. Keitel, T. Kuo, G. Mackenzie, M. McDonald, P. Schmor, Y. Yin, and D. Yuan. An ion source test stand for the ISAC facility at TRIUMF. *Nuclear Instruments and Methods in Physics Research Section B: Beam Interactions with Materials and Atoms*, 126(1):50 – 54, 1997.

[8] K. Floettmann. Some basic features of the beam emittance. *Physical Review Special Topics - Accelerators and Beams*, 6, 2003.

[9] T. Forrester. *Large Ion Beams: Fundamentals of generation and propagation*. Wiley-Interscience, 1988.

[10] U. Köster, O. Arndt, E. Bouquerel, V.N. Fedoseyev, H. Frånberg, A. Joinet, C. Jost, I.S.K. Kerkines, and R. Kirchner. Progress in ISOL target ion source

systems. *Nuclear Instruments and Methods in Physics Research Section B: Beam Interactions with Materials and Atoms*, 266(1920):4229 – 4239, 2008.

[11] E. Kugler. The ISOLDE facility. *Hyperfine Interactions*, 129(1):23–42, 2000.

[12] B. Laxdal. ARIEL top level requirements. TRIUMF Document-118534, 2016.

[13] M. A. Leitner, D. C. Wutte, and C. M. Lyneis. Design of the extraction system of the superconducting ecr ion source venus. In *Particle Accelerator Conference, 2001. PAC 2001. Proceedings of the 2001*, volume 1, pages 67–69 vol.1, 2001.

[14] T.I. Meyer. Five-year plan 2015-2020: Realizing the vision. TRIUMF, 2013.

[15] A. Mjøs. Adding standard solutions to targets. TRIUMF Document-102786, 2013.

[16] A. Sen, F. Ames, P. Bricault, J. Lassen, A. Laxdal, and A. Mjøs. Extraction and low energy beam transport from a surface ion source at the TRIUMF-ISAC facility. *Nuclear Instruments and Methods in Physics Research B*, 376, 2016.

[17] A. Shotter. Advances at ISOL facilities. *Nuclear Instruments and Methods in Physics Research Section B: Beam Interactions with Materials and Atoms*, 204:17 – 19, 2003.

[18] K. Siegbahn and R. Hellborg. *Electrostatic Accelerators: Fundamentals and Applications*. Springer Berlin Heidelberg, 2006.